



19990402 028

Band Structure Anisotropy in Semiconductor
Quantum Wells

THESIS

Steven J. Novotny, Captain, USAF
AFIT/ENP/GAP/99M-07

DEPARTMENT OF THE AIR FORCE
AIR UNIVERSITY
AIR FORCE INSTITUTE OF TECHNOLOGY

Wright-Patterson Air Force Base, Ohio

Approved for public release; distribution unlimited

AFIT/GAP/ENP/99M-07

Band Structure Anisotropy in Semiconductor Quantum Wells

THESIS

Steven J. Novotny
Captain

AFIT/GAP/ENP/99M-07

Approved for public release; distribution unlimited

The views expressed in this thesis are those of the author and do not reflect the official policy or position of the Department of Defense or the United States Government.

AFIT/GAP/ENP/99M-07

Band Structure Anisotropy in Semiconductor Quantum Wells

THESIS

Presented to the Faculty of the Graduate School of Engineering
of the Air Force Institute of Technology

Air University

In Partial Fulfillment of the
Requirements for the Degree of
Master of Science

Steven J. Novotny, BS

Captain

March 1999

Approved for public release; distribution unlimited

AFIT/ENP/GAP/99M-07

Band Structure Anisotropy in Semiconductor Quantum Wells

Steven J. Novotny, BS

Captain

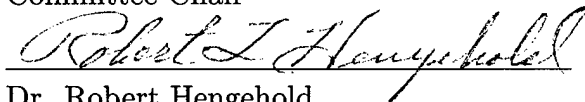
Approved:



Dr. David Weeks
Committee Chair

2 Mar 99

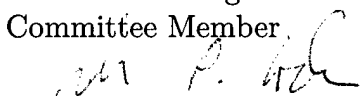
Date



Dr. Robert Hengehold
Committee Member

3 Mar 99

Date



Dr. John Loehr
Committee Member

3 MAR 99

Date

Preface

I would like to thank first my family for their patience and unconditional support. As with every endeavor in my life, this project would have been impossible and meaningless to accomplish without them. I would also like to thank my solid state physics instructor Dr. Robert Hengehold for being the first to present the true thrill and excitement of this field. Finally, I would like to thank my advisor Dr. David Weeks for not only being a guide to the world of physics, but also a true academic and intellectual mentor. His excitement for learning and teaching is unequalled.

Steven J. Novotny

Table of Contents

	Page
Preface	iii
List of Figures	vi
Abstract	viii
 I. Introduction	 1
1.1 Quantum Well Structures	2
1.2 Optical Absorption Properties	5
1.3 Anisotropy Analysis	6
1.4 Previous Work	6
 II. Theoretical Approach	 8
2.1 Bulk Material	8
2.1.1 $\mathbf{k} \cdot \mathbf{p}$ Theory	8
2.1.2 Coordinate System Transformation	10
2.1.3 Spin-Orbit Hamiltonian	11
2.1.4 $\mathbf{k} \cdot \mathbf{p}$ Hamiltonian	12
2.1.5 Strain Hamiltonian	13
2.1.6 Energy Level Band Structure for Bulk Material	16
2.2 Quantum Well	17
2.2.1 One Dimensional Square Well Problem (20)	17
2.2.2 Semiconductor Quantum Well	20
2.2.3 Quantum Well Dispersion Relationships	29

	Page
III. Computational Approach	30
3.1 Bulk Material Calculations	30
3.2 Quantum Well Calculations	30
3.2.1 Eigenvalues and Eigenvectors of $k_z(E)$	30
3.2.2 Determinant of Boundary Condition Matrix	37
3.3 Code Generation	42
IV. Results and Conclusions	44
4.1 Bulk Material Band Structures	44
4.2 Quantum Well Band Structures	46
4.3 Anisotropy	57
4.4 Summary and Recommendations	57
Appendix A. Subroutine Description	59
Appendix B. Values for Physical Constants	61
Bibliography	63
Vita	65

List of Figures

Figure		Page
1.	Growth layers in an AlGaAs/GaAs quantum well (19). . . .	2
2.	First Brillouin zone and symmetry points for zincblende and diamond structure (22).	3
3.	Energy levels and minibands in a multiple quantum well structure and a superlattice (19).	4
4.	Compensation for lattice mismatch in a strained material (2) .	15
5.	Bulk material dispersion relations for Si/Si ₇₀ Ge ₃₀ resulting from diagonalization of: (a) $H_{k,p} + H_{so}$ and (b) $H_{kp} + H_{so} + H_{strain}$	18
6.	One dimensional simple square well potential of width a . . .	21
7.	Definition of absolute valence band energy.	23
8.	Schematic of a bulk dispersion curve showing energy as a function of k_z and k_z as a function of energy (2).	31
9.	Positive real and positive imaginary values of kz for the lh , hh , and so bands.	34
10.	Positive real and positive imaginary values of kz for the lh , hh , and so bands. Note the joining of the lh and so bands at the point corresponding to the maximum energy in the lh band.	35
11.	All eigenvalues of the matrix describing kz as a function of energy.	36
12.	Plot of the determinant of the 30Å Si/SiGe quantum well boundary condition matrix vs. energy. $k_x=k_y=0$	37
13.	Plot of the determinant of the 30Å Si/SiGe quantum well boundary condition matrix vs. energy. $k_x=k_y=0$	38
14.	Graphical depiction of the secant method (21).	40
15.	Plot of the determinant of the 30Å Si/SiGe quantum well boundary condition matrix vs. energy.	41

Figure		Page
16.	Plot of the determinant of the 30Å Si/SiGe quantum well boundary condition matrix vs. energy.	42
17.	Bulk material dispersion curves for [001] strained GaAs. . .	44
18.	Bulk material dispersion curves for [001] strained In ₃₀ Ga ₇₀ As. . .	45
19.	Bulk material dispersion curves for [001] strained Si ₇₀ Ge ₃₀ . .	46
20.	Dispersion curves for [001] Al ₃₀ Ga ₇₀ As/GaAs quantum well with L=50 angstrom. Theta ranges from 0 (dark line) to 45 degrees in 10 degree increments (dashed lines).	48
21.	Dispersion curves for [110] Al ₃₀ Ga ₇₀ As/GaAs quantum well with L=50 angstrom. Theta ranges from 0 (dark lines) to 90 degrees in 10 degree increments (dashed lines).	49
22.	Dispersion curves for [001] In ₃₀ Ga ₇₀ As/GaAs quantum well with L=50 angstrom. Theta ranges from 0 (dark line) to 45 degrees in 10 degree increments (dashed lines).	50
23.	Dispersion curves for [110] In ₃₀ Ga ₇₀ As/GaAs quantum well with L=50 angstrom. Theta ranges from 0 (dark line) to 90 degrees in 10 degree increments (dashed lines).	51
24.	Dispersion curves for [001] Si/Si ₇₀ Ge ₃₀ quantum well with L=30 angstrom. Theta ranges from 0 (dark line) to 45 degrees in 10 degree increments (dashed lines).	52
25.	Dispersion curves for [110] Si/Si ₇₀ Ge ₃₀ quantum well with L=30 angstrom. Theta ranges from 0 (dark line) to 90 degrees in 10 degree increments (dashed lines).	53
26.	Surface plot of the bandstructure for [001] Al ₃₀ Ga ₇₀ As/GaAs quantum well with L=50 angstrom.	54
27.	Surface plot of the bandstructure for [001] GaAs/In ₃₀ Ga ₇₀ As quantum well with L=50 angstrom.	55
28.	Surface plot of the bandstructure for [001] Si/Si ₇₀ Ge ₃₀ quantum well with L=30 angstrom.	56

Abstract

The focus of this research is an investigation of energy band anisotropy in simple quantum well structures. This anisotropy results from the asymmetry of the periodic potential within the crystal lattice. For sufficiently high doping levels, band structure anisotropy is expected to play an important role in the evaluation of the electronic and optical properties of the quantum well structures. The analysis uses a model based on a 6×6 Luttinger-Kohn $\mathbf{k} \cdot \mathbf{p}$ approach for bulk material valence band structure together with the Envelope Function approximation. The model is used to analyze Si/Si_{1-x}Ge_x, GaAs/Al_xGa_{1-x}As, and GaAs/In_xGa_{1-x}As quantum wells for the [110] and the [001] growth directions. The resulting bandstructures show significant anisotropy for materials grown in both the [110] and [001] growth directions. In all cases the materials grown in the [110] direction show a more pronounced anisotropy than the materials grown in the [001] directions. For the [001] growth directions, the bandstructures were effectively isotropic for values of k_{\parallel} less than $0.4 \text{ Angstrom}^{-1}$ for Si/Si₇₀Ge₃₀, $0.6 \text{ Angstrom}^{-1}$ for GaAs/Al₃₀Ga₇₀As, and $0.5 \text{ Angstrom}^{-1}$ for GaAs/In₃₀Ga₇₀As.

Band Structure Anisotropy in Semiconductor Quantum Wells

I. Introduction

Since the inception of the semiconductor quantum well in 1970 by Esaki and Tsu (12) and the later advances in Molecular Beam Epitaxy (MBE) and Metal-Organic Chemical Vapor Deposition (MOCVD), quantum well devices have proven to be very useful in the field of optoelectronics. Two significant devices in which these structures are used are the laser diode and the infrared photodetector (15).

Of particular interest to the Air Force is the use of these bandgap-engineered materials in infrared photodetectors in the wavelength range corresponding to the atmospheric windows of $3\text{-}5\mu\text{m}$ and $8\text{-}14\mu\text{m}$ for use in applications such as thermal imaging, guidance, and reconnaissance (2),(16). Quantum well photodetectors are also well suited for use in the $1.3\mu\text{m}$ and $1.5\mu\text{m}$ range which makes them useful for fiber-optic communications (15).

Quantum devices offer many advantages over normal photodetectors. First they have a great flexibility in design which allows tailoring to a specific operating wavelength. As explained in the next section, parameters such as well width and alloy composition can be modified to change the quantum well energy levels which in turn change the optical response. Second, for inter-subband transitions quantum well devices have a narrow pass-band spectral response. This is a result of the well possessing a limited number of energy levels between which transitions can occur (15). Finally, by using materials such as Si/SiGe, operating temperatures can be raised to approximately 75K from that required by bulk material detectors, which is in the region of 30K (2).

AlGaAs	GaAs	AlGaAs	GaAs	AlGaAs	GaAs	AlGaAs	GaAs Substrate
--------	------	--------	------	--------	------	--------	----------------

Figure 1 Growth layers in an AlGaAs/GaAs quantum well (19).

1.1 Quantum Well Structures

Analysis of the optical properties for a material typically requires knowledge of the material's bandstructure. The bandstructure can be modified by creating heterostructures which are discontinuities in the crystal created by placing two different materials in contact (10). The particular heterostructure studied in this research is the quantum well. The bandstructure of the quantum well in most cases is very different from that found in the bulk material.

Semiconductor quantum wells are created by alternating semiconductor materials with differing bandgaps. Through approaches like MBE, very thin layers are created which approach the deBroglie wavelength of the electron. This allows for quantum confinement effects to become important. The growth layers for a GaAs/AlGaAs multiple quantum well are shown in figure 1.

In crystal structures the periodicity created by the particular atomic arrangement creates energy bands that determine the electronic properties of the material. This bandstructure identifies the allowed energy eigenstates for a particular value of the wave vector \mathbf{k} . The bandstructure is commonly displayed as a function of direction in k -space from one symmetry point to another within the Brillouin zone. The Brillouin zone is defined as a single unit cell of the reciprocal lattice. Examples of some symmetry points and the first Brillouin zone for the zincblende crystal structure are shown in figure 2.

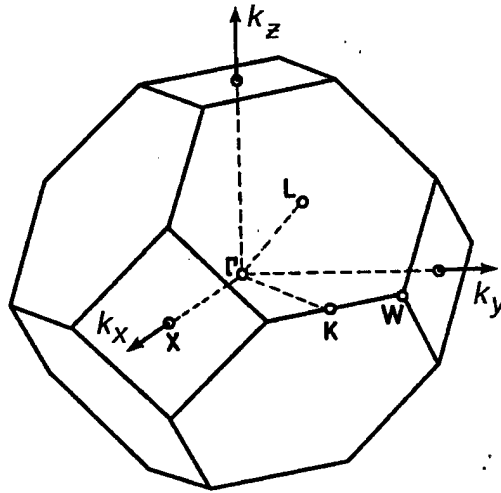
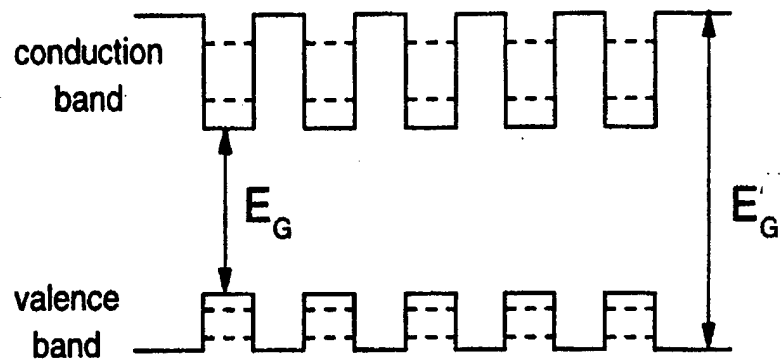


Figure 2 First Brillouin zone and symmetry points for zincblende and diamond structure (22).

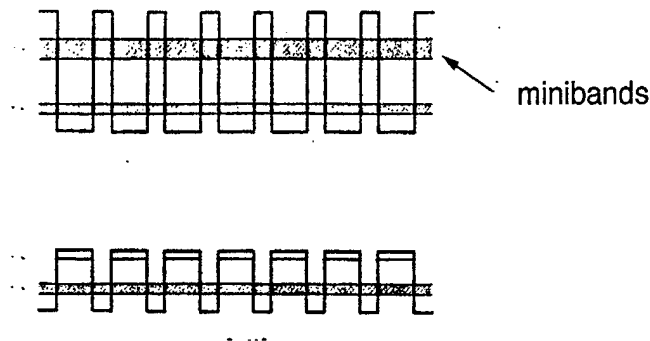
In a quantum well, the bandstructure can be modified to optimize the optical properties of the device. Well width, growth direction, and alloy composition can be varied to maximize absorption for a particular wavelength. Also, by creating multiple wells of different widths and/or compositions a detector can respond to multiple wavelengths(2).

Quantum well devices are usually comprised of many quantum wells and, depending on the spacing between the individual wells, are divided into two categories: superlattices or multiple quantum well structures. If the spacing between the individual wells is small enough such that the wavefunctions of the confined carriers interact with the wavefunctions of those carriers in the neighboring wells, then a superlattice is formed. If the spacing between wells is great enough such that there is essentially no interaction between wavefunctions of neighboring wells, then the structure is considered a multiple quantum well. The two types of structures are shown in figure 3.

In the case of superlattices, the overlap of wavefunctions causes a splitting of the degenerate energy levels in the neighboring quantum wells. This splitting of discrete energy levels results in the creation of minibands. The minibands consist of



Multiple Quantum Well



Superlattice

Figure 3 Energy levels and minibands in a multiple quantum well structure and a superlattice (19).

a number of individual bands equal to the number of wells in the superlattice (15). The presence of minibands allows a variety of transitions to occur corresponding to different wavelengths.

In the case of multiple quantum well structures, the lack of wavefunction overlap leaves the energy levels discrete. This also allows an increase in the optical absorption of the device by a factor equal to the number of wells in the structure. However, 'effective minibands' will also form in a multiple quantum well structure due to slight variations in well widths or alloy composition (15). This results in

slightly different energy levels in each of the quantum wells making up the multiple quantum well structure.

1.2 Optical Absorption Properties

The foundation of optoelectronic devices lies in the interaction between incident electromagnetic radiation and electrons or holes in the detector material. This interaction can be described by the absorption coefficient α ($\alpha < 0$ for gain material and $\alpha > 0$ for attenuating material). Absorption occurs when a photon assisted transition occurs; an electron gaining energy from a photon and moving from one energy level to another.

The form of the linear absorption coefficient used by Green (1) can be expressed as

$$\alpha \propto \int dk_{\parallel} \frac{f(P_{mn}(k_{\parallel}))}{E_n(k_{\parallel}) - E_m(k_{\parallel})} \quad (1)$$

where P_{mn} is the momentum matrix elements for transitions between states n and m and E_n and E_m correspond to the energy levels of the initial and final states. Both the energy and the momentum vector are functions of k_{\parallel} and must be evaluated at each value of k_{\parallel} for which the integral must be performed. The integral in equation 1 is performed through the region of k -space dictated by the Fermi level.

A common way to calculate absorption coefficients is to perform a calculation of the quantum well band structure and momentum matrix elements for one direction in k -space. In many cases, the assumption that the band structure is isotropic throughout the plane is made and the simple factor of 2π is utilized. However, the band structure is not isotropic throughout the plane of the quantum well. Therefore, to accurately model absorption coefficients the magnitude of the anisotropy must be determined and considered in any calculation.

1.3 Anisotropy Analysis

There are several models used for calculating the bandstructures for semiconductor materials. The most common are the nearly free electron model, the tight-binding method and the one used in this analysis, the $\mathbf{k} \cdot \mathbf{p}$ method (17). The nearly-free-electron model assumes free electrons interacting weakly with the positive ions in the lattice. Due to Bragg reflection forbidden energy zones occur, i.e. bandgaps develop. In the tight-binding model, electronic wave functions are assumed to be comprised of hydrogenic wavefunctions which are localized at the lattice sites. The potential is described by Coulombic potentials of the nearest neighbors only. Though the tight-binding model is considered the most accurate, it is computationally intensive. The final method uses the $\mathbf{k} \cdot \mathbf{p}$ model which will be described in detail in chapter 2. This is a semi-empirical method based on experimentally measured quantities.

1.4 Previous Work

Over the past five years modeling of the absorption spectra of quantum well structures has been the subject of two graduate research projects at the Air Force Institute of Technology (AFIT) (2). Mathematical models have been developed and experimental data has been taken for Si/SiGe quantum well structures. These models allow calculation of energy levels in the quantum well and the absorption coefficients corresponding to bound-to-bound valence band transitions. The calculations were based on the band structure corresponding to a single azimuthal direction in the plane of the quantum well and the assumption of band structure isotropy.

As discussed earlier, the calculation of the absorption coefficients requires an integration of the energy bands throughout the plane of the quantum well. This requires a calculation of the band structure for each incremental step in the azimuthal angle theta. This research reproduces the mathematical models of the

quantum well structure developed by Gregg (2) in FORTRAN code and allows enhanced analysis of the band structure and the associated anisotropy.

The remainder of this document presents the theory and the computational approach used to determine the band structure in a semiconductor quantum well. First, bulk material band structures are calculated using the Luttinger-Kohn $\mathbf{k} \cdot \mathbf{p}$ theory including spin-orbit interaction effects. The strain Hamiltonian developed by Kleiner and Roth, presented later by Hasegawa (4) and then by People and Jackson (8) is also incorporated. Second, the analysis for the quantum well is presented. Quantum well valence band offsets are based on model solid theory of Van De Walle as presented by People and Jackson (8). The Envelope Function approximation as presented by Szmulowicz (6) is used to determine the quantum well band structure. The FORTRAN programs necessary to perform the required calculations are also summarized and discussed. Finally the resulting dispersion curves for the quantum well are presented for various azimuthal angles through the plane of the quantum well. Materials considered are Si/Si_{1-x}Ge_x , GaAs/Al_xGa_{1-x}As , and GaAs/In_xGa_{1-x}As.

II. Theoretical Approach

This chapter discusses in general the approach taken in determining the band structure for a semiconductor quantum well. Section 2.1 describes the development of the total Hamiltonian for the bulk material and how bulk material bandstructures are determined from the eigenvalues of the Hamiltonian matrix. Section 2.2 discusses the use of the Envelope Function Approximation (EFA) in the modeling of the semiconductor quantum well and compares its development and solution to that of the one-dimensional square well problem solved in basic quantum mechanics.

2.1 Bulk Material

The determination of energy levels in a bulk material semiconductor is accomplished by solving the time-independent Schrodinger equation.

$$\hat{H}\psi = E\psi \quad (2)$$

The general form for the bulk material Hamiltonian is comprised of several terms. These are the $\mathbf{k} \cdot \mathbf{p}$ Hamiltonian $H_{k \cdot p}$, the spin-orbit Hamiltonian H_{so} , and the strain Hamiltonian H_{strain} .

2.1.1 $\mathbf{k} \cdot \mathbf{p}$ Theory. Electrons and holes in a periodic potential such as a crystal lattice obey Bloch's Theorem. Bloch's theorem states that wavefunctions in a periodic potential can be expressed as the product of a function having the periodicity of the lattice and a plane wave.

The general form for such a function can be expressed as

$$\psi_{n\mathbf{k}}(\mathbf{r}) = e^{i\mathbf{k} \cdot \mathbf{r}} u_{n\mathbf{k}}(\mathbf{r}) \quad (3)$$

where u is a function with the periodicity of the lattice. Substituting this into the one-electron Schrodinger equation

$$\left[\frac{\mathbf{p}^2}{2m} + V(\mathbf{r}) \right] \psi_{n\mathbf{k}} = E_n(\mathbf{k}) \psi_{n\mathbf{k}} \quad (4)$$

and assuming a periodic potential will give the general $\mathbf{k} \cdot \mathbf{p}$ equation(7)

$$\left[\frac{\mathbf{p}^2}{2m} + \frac{\hbar \mathbf{k} \cdot \mathbf{p}}{m} + \frac{\hbar^2 k^2}{2m} + V(\mathbf{r}) \right] u_{n\mathbf{k}}(\mathbf{r}) = E_n(\mathbf{k}) u_{n\mathbf{k}}(\mathbf{r}) \quad (5)$$

Bloch functions of the form in equation 3 create a complete set of basis functions for any value of \mathbf{k} . One possibility used by Luttinger and Kohn is based on Bloch functions at zone center, $\mathbf{k} = 0$ (3). Following an approach outlined by Kane (18), $u_{n\mathbf{k}}(\mathbf{r})$ in equation 5 can be expressed in the $\mathbf{k} \cdot \mathbf{p}$ representation by

$$u_{n\mathbf{k}}(\mathbf{r}) = \sum_{n'} c_{n'n} u_{n'\mathbf{k}_0}(\mathbf{r}) \quad (6)$$

Multiplying both sides of equation 5 by $u_{n\mathbf{k}_0}(\mathbf{r})$, replacing $u_{n\mathbf{k}}(\mathbf{r})$ with the form given in equation 6, and integrating gives

$$\sum_{n'} \left\{ \left[E_n(\mathbf{k}_0) + \frac{\hbar^2 k^2}{2m} \right] \delta_{nn'} + \frac{\hbar}{m} \mathbf{k} \cdot \mathbf{p}_{n'n} \right\} c_{n'n} = E_n(\mathbf{k}) c_{nn} \quad (7)$$

The term $\mathbf{p}_{n'n}$ is given by

$$\mathbf{p}_{n'n} = \int u_{n\mathbf{k}_0}^*(\mathbf{r}) \mathbf{p} u_{n'\mathbf{k}_0}(\mathbf{r}) d\mathbf{r} \quad (8)$$

where the integral is over the unit cell and \mathbf{p} is the momentum operator given by

$$\mathbf{p} = -i\hbar \nabla \quad (9)$$

Using an application of perturbation theory for small \mathbf{k} to solve equation 7, Luttinger and Kohn derived the general form for the Hamiltonian describing electron or hole behavior in a periodic potential (3). However, the momentum matrix elements given in equation 8 are difficult to calculate because they require specific knowledge of the Bloch functions. A more manageable expression of the Hamiltonian uses angular momentum operators and inverse mass parameters known as Luttinger coefficients (2). By using these experimentally measured values, the calculation of the momentum matrix elements, $\mathbf{p}_{n'n}$, of equation 10 are avoided. Using these values, the Hamiltonian can be expressed as

$$H_{\mathbf{k},\mathbf{p}} = -\frac{\hbar^2}{2m} \left(2\gamma_1 (k_{xx} + k_{yy} + k_{zz}) \hat{1} \right) \quad (10)$$

$$-12\gamma_2 \left(\left(\hat{L}_x^2 - \frac{1}{3} \hat{L}^2 \right) k_{xx} + c.p. \right) - 24\gamma_3 \left(\left(\hat{L}_{xx} \right) k_{xy} + c.p. \right)$$

where γ 's are the empirically determined Luttinger coefficients and *c.p.* is a cyclic permutation in x , y , and z . Equation 10 gives three doubly degenerate energy bands in the dispersion relationship which are degenerate at zone center. The three bands are labeled heavy hole, light hole, and split off based on their corresponding effective masses.

2.1.2 Coordinate System Transformation. Since the previous equations have been developed using symmetry based coordinates, a transformation must be done to align the coordinate system with the direction of interest. This is done through the use of a rotation matrix based on euler angles applied to both the angular momentum operators and the wave vectors (1).

The transformation is given as

$$\begin{pmatrix} \hat{L}_{x'} \\ \hat{L}_{y'} \\ \hat{L}_{z'} \end{pmatrix} = R \cdot \begin{pmatrix} \hat{L}_x \\ \hat{L}_y \\ \hat{L}_z \end{pmatrix} \quad (11)$$

$$\begin{pmatrix} k_{x'} \\ k_{y'} \\ k_{z'} \end{pmatrix} = R \cdot \begin{pmatrix} k_x \\ k_y \\ k_z \end{pmatrix} \quad (12)$$

where R is given by

$$R = \begin{pmatrix} \cos \theta \cos \phi & -\sin \phi & \sin \theta \cos \phi \\ \cos \theta \sin \phi & \cos \phi & \sin \theta \sin \phi \\ -\sin \theta & 0 & \cos \theta \end{pmatrix} \quad (13)$$

The values for θ and ϕ are based upon the direction of crystal growth. For the [110] direction $\theta = \frac{\pi}{2}$ and $\phi = \frac{\pi}{4}$. For the [001] direction $\theta = 0$ and $\phi = \frac{\pi}{4}$.

2.1.3 Spin-Orbit Hamiltonian. Diagonalizing the form of the Hamiltonian given in equation 10 results in a six fold degeneracy at zone center. If the interaction between the electron's spin and orbital angular momentum is incorporated, the degeneracy will be partially removed. Terms describing the spin-orbit induced

perturbations are diagonal elements in the $|j, m_j, \mathbf{k}\rangle$ basis and are given by

$$H_{so} = \begin{pmatrix} 0 & 0 & 0 & 0 & 0 & 0 \\ 0 & 0 & 0 & 0 & 0 & 0 \\ 0 & 0 & 0 & 0 & 0 & 0 \\ 0 & 0 & 0 & 0 & 0 & 0 \\ 0 & 0 & 0 & 0 & -\Delta & 0 \\ 0 & 0 & 0 & 0 & 0 & -\Delta \end{pmatrix} \quad (14)$$

where Δ is the experimentally measured spin-orbit interaction term, $j = \frac{3}{2}$, $m_j = \frac{3}{2}, \frac{1}{2}, -\frac{1}{2}, -\frac{3}{2}$ and $j = \frac{1}{2}$, $m_j = \frac{1}{2}, -\frac{1}{2}$.

2.1.4 $\mathbf{k} \cdot \mathbf{p}$ Hamiltonian. Performing the transformation described in section 2.1.2 results in the following form for the bulk material $\mathbf{k} \cdot \mathbf{p}$ Hamiltonian in the $|j, m_j, \mathbf{k}\rangle$ basis:

$$H_{\mathbf{k} \cdot \mathbf{p}} = -\frac{\hbar^2}{2m_o} \begin{pmatrix} hh & \alpha & \beta & 0 & i\frac{\alpha}{\sqrt{2}} & -i\beta\sqrt{2} \\ \alpha^* & lh & 0 & \beta & i\frac{\delta}{\sqrt{2}} & i\alpha\sqrt{\frac{3}{2}} \\ \beta^* & 0 & lh & -\alpha & -i\alpha^*\sqrt{\frac{3}{2}} & i\frac{\delta}{\sqrt{2}} \\ 0 & \beta^* & -\alpha^* & hh & -i\beta^*\sqrt{2} & -i\frac{\alpha^*}{\sqrt{2}} \\ i\frac{\alpha}{\sqrt{2}} & -i\frac{\delta}{\sqrt{2}} & i\alpha\sqrt{\frac{3}{2}} & i\beta\sqrt{2} & so & 0 \\ i\beta^*\sqrt{2} & -i\alpha^*\sqrt{\frac{3}{2}} & -i\frac{\delta}{\sqrt{2}} & i\frac{\alpha}{\sqrt{2}} & 0 & so \end{pmatrix} \quad (15)$$

For the [001] growth direction:

$$hh = (k_x^2 + k_y^2 + k_z^2)\gamma_1 + (k_x^2 + k_y^2 - 2k_z^2)\gamma_2 \quad (16a)$$

$$lh = (k_x^2 + k_y^2 + k_z^2)\gamma_1 - (k_x^2 + k_y^2 - 2k_z^2)\gamma_2 \quad (16b)$$

$$so = (k_x^2 + k_y^2 + k_z^2)\gamma_1 \quad (16c)$$

$$\alpha = -2i\sqrt{3}(k_x - ik_y)k_z\gamma_3 \quad (16d)$$

$$\beta = \sqrt{3}((k_x^2 - k_y^2)\gamma_2 - 2ik_xk_y\gamma_3) \quad (16e)$$

$$\delta = lh - hh \quad (16f)$$

For the [110] growth direction:

$$hh = (k_x^2 + k_y^2 + k_z^2)\gamma_1 - (k_x^2 - 2k_y^2 + k_z^2)\frac{\gamma_1}{2} + (k_x^2 - k_z^2)\frac{3}{2}\gamma_3 \quad (16g)$$

$$lh = (k_x^2 + k_y^2 + k_z^2)\gamma_1 + (k_x^2 - 2k_y^2 + k_z^2)\frac{\gamma_1}{2} - (k_x^2 - k_z^2)\frac{3}{2}\gamma_3 \quad (16h)$$

$$so = (k_x^2 + k_y^2 + k_z^2)\gamma_1 \quad (16i)$$

$$\alpha = -2i\sqrt{3}(k_x\gamma_2 - ik_y\gamma_3)k_z \quad (16j)$$

$$\beta = \frac{\sqrt{3}}{2}((k_x^2 - 2k_y^2 + k_z^2)\gamma_2 + (k_x^2 - 4ik_xk_y - k_z^2)\gamma_3) \quad (16k)$$

$$\delta = lh - hh \quad (16l)$$

2.1.5 Strain Hamiltonian. When two materials having different lattice constants are used to create a heterostructure, strain will be induced into the material as a result of the necessary compensation for the lattice mismatch. This perturbation to the symmetry of the periodic potential changes the energy levels in such a way as to cause a splitting in the degeneracy of the light hole and heavy hole bands. The Hamiltonian describing the effect of strain is given in terms of orbital angular momentum operators; deformation potentials, D_1 , D_2 , and D_3 ; and

strain tensor components $e_{\alpha\beta}$ (2),

$$H_{strain} = D_1 (e_{xx} + e_{yy} + e_{zz}) \hat{I} + 2D_2 \left[\left(\hat{L}_x^2 - \frac{1}{3} \hat{L}^2 \right) e_{xx} + c.p. \right] + 2D_3 \left[\left(\hat{L}_{xy} \right) e_{xy} + c.p. \right] \quad (17)$$

where *c.p.* denotes cyclic permutation. The first term of equation 17 represents a shift in average energy of the valence band. Therefore, this term is excluded from bulk calculations since absolute values of energy are not an issue. However, in the quantum well band structure calculations, where absolute or relative energy values are important, this term is incorporated.

Performing a rotation operation on the angular momentum operators of equation 17 together with a similarity transformation of the strain tensor similar to that done earlier for $H_{\mathbf{k},\mathbf{p}}$, yields the strain Hamiltonian where the D_1 term in equation 17 has been omitted

$$H_{strain} = \begin{pmatrix} e_2 & 0 & e_3 & 0 & 0 & -ie_3\sqrt{2} \\ 0 & -e_2 & 0 & e_3 & -ie_2\sqrt{2} & 0 \\ e_3 & 0 & -e_2 & 0 & 0 & -ie_2\sqrt{2} \\ 0 & e_3 & 0 & e_2 & -ie_3\sqrt{2} & 0 \\ 0 & ie_2\sqrt{2} & 0 & ie_3\sqrt{2} & 0 & 0 \\ ie_3\sqrt{2} & 0 & ie_2\sqrt{2} & 0 & 0 & 0 \end{pmatrix} \quad (18)$$

For the [001] growth direction:

$$e_2 = \frac{2}{3} D_2 (e_{zz} - e_{xx}) \quad (19a)$$

$$e_3 = 0 \quad (19b)$$

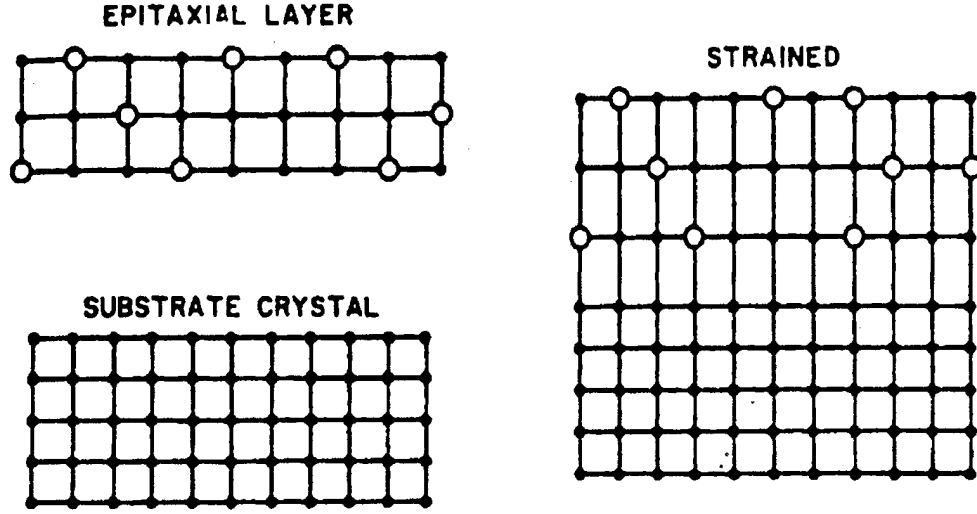


Figure 4 Compensation for lattice mismatch in a strained material (2) .

For the $[110]$ growth direction:

$$e_2 = -\frac{1}{3}D_2(e_{zz} - e_{xx}) + \frac{1}{2}D_3e_{xy} \quad (20a)$$

$$e_3 = -\frac{1}{\sqrt{3}}D_2(e_{xx} - e_{zz}) + \frac{1}{2\sqrt{3}}D_3e_{xy} \quad (20b)$$

The values for D_i are based on linear interpolation of the deformation potentials for the alloy's constituents. D_1 is the interpolated value of the hydrostatic deformation potentials a_v , D_2 is the interpolated value of D_u , the valence-band deformation potential for uniaxial stress in the $[001]$ direction, and D_3 is the interpolated value of D'_u , the valence band deformation potential for uniaxial stress in the $[111]$ direction.

The values $e_{\alpha\beta}$ are conventional strain components and can be expressed in terms of the unique elements of the stiffness matrix C for cubic structures and the value for in-plane strain $[(8),(7)]$. The in-plane strain is a function of the lattice

constants in the well and the barrier material and can be expressed as

$$e_{\parallel} = \frac{a_s}{b} - 1 \quad (21)$$

where b is the unstrained lattice constant and a_s is the lattice constant of the substrate or barrier material. This represents the percentage change in the lattices constant (7).

The expressions for the strain components are (8)

for the [001] growth direction:

$$\begin{aligned} e_{xx} &= e_{\parallel} \\ e_{xy} &= 0 \\ e_{zz} &= -e_{\parallel} \left(\frac{2C_{12}}{C_{11}} \right) \end{aligned} \quad (22)$$

for the [110] growth direction:

$$\begin{aligned} e_{xx} &= e_{\parallel} \left[\frac{2C_{44} - C_{12}}{2C_{44} + C_{11} + C_{12}} \right] \\ e_{xy} &= -e_{\parallel} \left[\frac{2[C_{11} - 2C_{12}]}{2C_{44} + C_{11} + C_{12}} \right] \\ e_{zz} &= e_{\parallel} \end{aligned} \quad (23)$$

2.1.6 Energy Level Band Structure for Bulk Material. The Hamiltonian for unstrained bulk material can now be written as $H_{total} = H_{k \cdot p} + H_{so}$ and the Hamiltonian for strained bulk material can be written as $H_{total} = H_{k \cdot p} + H_{so} + H_{strain}$. Both expressions are functions of $\mathbf{k} = (k_x, k_y, k_z) = (k_z, \mathbf{k}_{\parallel})$ and empirically derived or tabulated data specific to the constituent elements. These constants are listed in appendix B. Using the approach by Gregg (2), the values used in the calculation for an alloy material are linearly interpolated values based on the percentage composition of one material in the other. For example, the Luttinger

coefficients in an alloy of Silicon and Germanium are given as

$$\gamma = \gamma_{\text{Si}} + x(\gamma_{\text{Ge}} - \gamma_{\text{Si}}) \quad (24)$$

where x is the percentage of Germanium in the alloy.

Diagonalizing the appropriate Hamiltonian gives the energy values for the bulk material as a function of \mathbf{k} . In an unstrained material, there will be two bands at zone center, one being doubly degenerate, the other being quadruply degenerate. The doubly degenerate band is the split off band and the quadruply degenerate bands at zone center are the light hole and heavy hole bands. The bands are named for their effective masses and their relative location as a function of energy. In strained material there will be three doubly degenerate bands. This is a result of the light hole and heavy hole bands splitting due to the strain perturbation. Examples of the bandstructure are shown in figure 5 for Si/Si₇₀Ge₃₀ alloy.

2.2 Quantum Well

The approach used in determining the energy eigenstates within a semiconductor quantum well structure is similar to that used in determining the eigenstates for a one dimensional square well potential. This section first revisits the one dimensional square well potential and then explains, in an analogous manner, the solution to the semiconductor quantum well problem.

2.2.1 One Dimensional Square Well Problem (20). Recalling the simple one dimensional square well problem, one starts with the time independent Schrodinger equation

$$\left[\frac{\mathbf{p}^2}{2m} + V(z) \right] \psi = E\psi \quad (25)$$

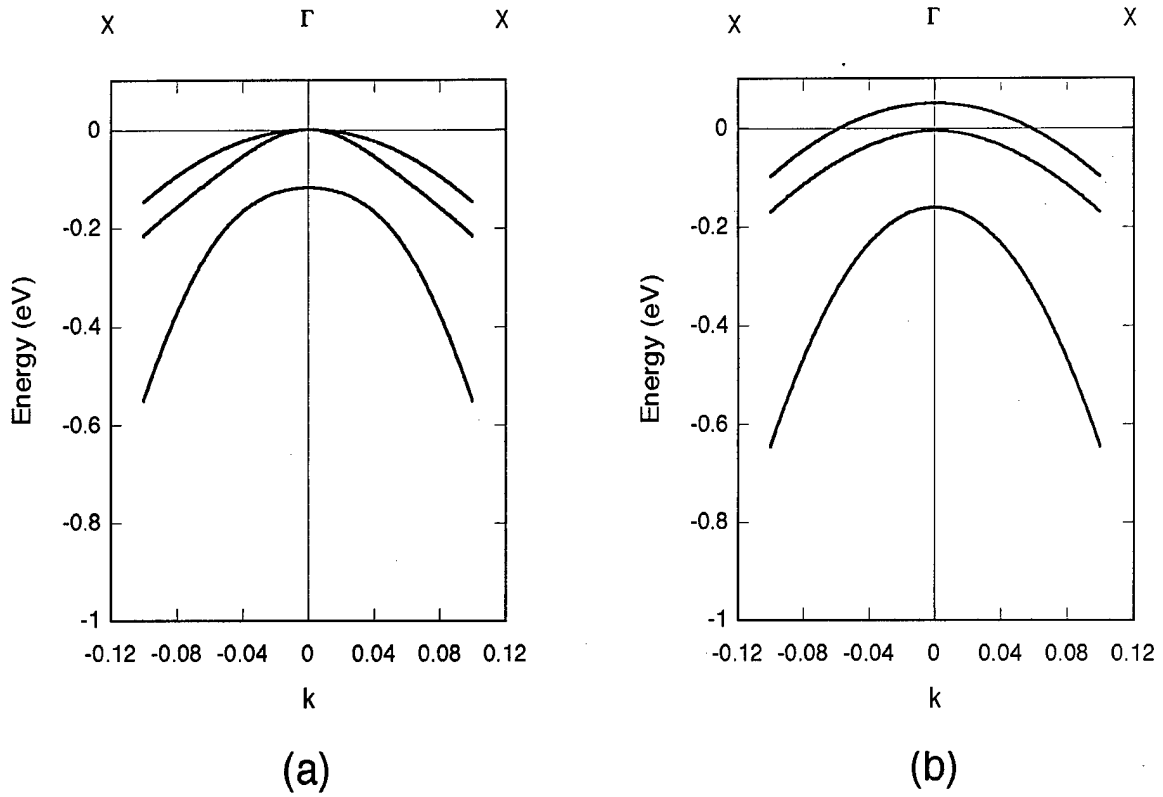


Figure 5 Bulk material dispersion relations for Si/Si₇₀Ge₃₀ resulting from diagonalization of: (a) $H_{k,p} + H_{so}$ and (b) $H_{k,p} + H_{so} + H_{strain}$

where \mathbf{p} is the momentum operator given as

$$\mathbf{p} = -i\hbar \frac{\partial}{\partial z} \quad (26)$$

Next the wave functions are assumed to be linear combinations of plane waves of the form

$$\psi(z)_{left} = Ae^{k_b z} + Be^{-k_b z} \quad (27a)$$

$$\psi(z)_{well} = Ce^{ik_w z} + De^{-ik_w z} \quad (27b)$$

$$\psi(z)_{right} = Ee^{k_b z} + Fe^{-k_b z} \quad (27c)$$

Using this form for the wave functions in the Schrodinger equation given in equation 25, values for the wave vector k can be expressed as a function of energy E . The expressions for k in the well and barrier of a simple square well potential are

$$k_w = \frac{\sqrt{2mE}}{\hbar} \quad (28a)$$

$$k_b = \frac{\sqrt{2m(V_0 - E)}}{\hbar} \quad (28b)$$

Since the wave functions are utilized to describe the behavior of observables such as position, momentum, etc., boundary conditions must be placed on the wave functions at the well/barrier interface to ensure both the wave functions and their derivatives are well behaved. These boundary conditions are

$$\psi\left(\pm\frac{a}{2}\right)_b = \psi\left(\pm\frac{a}{2}\right)_w \quad (29a)$$

$$\frac{\partial}{\partial z}\psi(z)|_{z=\pm\frac{a}{2}} = \frac{\partial}{\partial z}\psi(z)|_{z=\pm\frac{a}{2}} \quad (29b)$$

An addition boundary condition placed on the wave functions is that they must decay to zero as z approaches $\pm\infty$. This requires the coefficients B and E to be equal to zero. Using these boundary conditions at the barrier/well interface, a

system of equations can be developed and expressed as

$$Ce^{-ik_w(\frac{a}{2})} + De^{ik_w(\frac{a}{2})} = Ae^{-k_b(\frac{a}{2})} \quad (30a)$$

$$Ce^{ik_w(\frac{a}{2})} + De^{-ik_w(\frac{a}{2})} = Fe^{-k_b(\frac{a}{2})} \quad (30b)$$

$$ik_w Ce^{-ik_w(\frac{a}{2})} - ik_w De^{ik_w(\frac{a}{2})} = k_b Ae^{-k_b(\frac{a}{2})} \quad (30c)$$

$$ik_w Ce^{ik_w(\frac{a}{2})} - ik_w De^{-ik_w(\frac{a}{2})} = -k_b Fe^{-k_b(\frac{a}{2})} \quad (30d)$$

This system of equations can be represented by a matrix equation of the following form

$$\begin{pmatrix} e^{-ik_w(\frac{a}{2})} & e^{-ik_w(\frac{a}{2})} & -e^{-k_b(\frac{a}{2})} & 0 \\ e^{-ik_w(\frac{a}{2})} & e^{-ik_w(\frac{a}{2})} & 0 & -e^{-k_b(\frac{a}{2})} \\ ik_w e^{-ik_w(\frac{a}{2})} & -ik_w e^{-ik_w(\frac{a}{2})} & -k_b e^{-k_b(\frac{a}{2})} & 0 \\ ik_w e^{-ik_w(\frac{a}{2})} & -ik_w e^{-ik_w(\frac{a}{2})} & 0 & k_b e^{-k_b(\frac{a}{2})} \end{pmatrix} \begin{pmatrix} C \\ D \\ A \\ F \end{pmatrix} = \begin{pmatrix} 0 \\ 0 \\ 0 \\ 0 \end{pmatrix} \quad (31)$$

or more simply

$$[M] \cdot \chi = 0 \quad (32)$$

This can only be true, assuming non-trivial elements of χ , if

$$\det [M] = 0 \quad (33)$$

The matrix M is a function of k which is a function of energy E . Thus an expression for $\det [M]$ as a function of energy can be derived and the roots found with a numerical root finding tool. These roots correspond to the energy eigenvalues of the system.

2.2.2 Semiconductor Quantum Well. The reason for the simplicity of the calculation in the simple square well problem is that k can be found easily

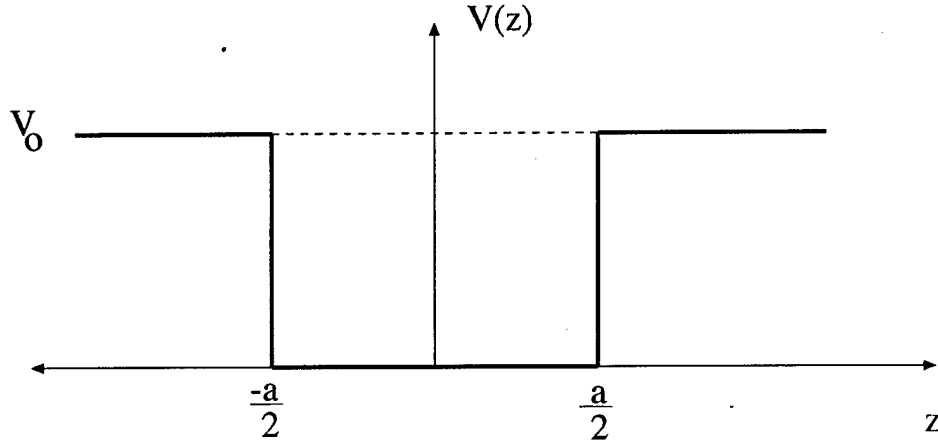


Figure 6 One dimensional simple square well potential of width a .

as a function of energy. For the case of semiconductor quantum well structures this relationship cannot be expressed analytically. Therefore a method must be developed to invert the expressions found in the previous chapter from $E(\mathbf{k})$ to $\mathbf{k}(E)$ or more precisely $k_z(E, \mathbf{k}_{\parallel})$. This is accomplished through a method presented by Szmulowicz which expands the Hamiltonian in powers of k_z and develops an eigenvalue problem from which k_z can be found for a particular set of values for energy E and a particular value for \mathbf{k}_{\parallel} (6). This process is explained in section 2.2.2.2.

Once the values for k_z are known, they can be incorporated into a matrix equation of the form shown in equation 33 to see if the determinant is equal to zero. Recall that the matrix was developed from the application of boundary conditions to the well and barrier wave functions. If the determinant is equal to zero, then the values of E are in fact eigenvalues for the system. Using this approach, dispersion relationships can be developed for the quantum well structure. This process is explained in sections 2.2.2.3 through 2.2.2.4.

2.2.2.1 Valence Band Energy Offset. For the bulk material calculations in the previous section of this chapter, absolute values for energy were not considered. The only objective was to present the bands relative to one another.

However, for the calculation of the quantum well it is necessary to predict not only an absolute value for the bands but also the difference or offset between bands in the barrier and the well material. This is analogous to the depth of the potential well in the one dimensional problem.

The approach taken for this model uses an average valance band energy E_{av}^v based on model solid theory of Van De Walle and presented by People and Jackson (8). Model-solid theory was developed to estimate the electrostatic potential difference across a heterojunction. The value of E_{av}^v corresponds to the average energy at the top of the valence band, ignoring spin-orbit interaction effects. Using this basis to establish an absolute scale, the average energy for the valence band in a material is a function of three values: the average valence band energy E_{av}^v found through model solid theory; the magnitude of the spin-orbit term Δ ; and the shift in the average energy due to crystal strain.

The first two values can be found tabulated (8). The shift due to the strain is calculated from tabulated data and is a function of an alloy's stoichiometry. The shift in the average valence band energy due to strain is

$$e_1 = D_1(2e_{xx} + e_{zz}) \quad (34)$$

where D_1 is a constant based on linear interpolation of the hydrostatic deformation potentials a_v for the two elements in the alloy. The expressions for e_{xx} and e_{zz} were given earlier in equations 22 and 23.

Mathematically, the offset is incorporated by adding a constant to both the well Hamiltonian and the barrier Hamiltonian. Therefore the total Hamiltonians are expressed as

$$H_{total}^b = H_{k,p} + H_{so} + V_b - E_{shift} \quad (35a)$$

$$H_{total}^w = H_{k,p} + H_{so} + H_{strain} + V_w - E_{shift} \quad (35b)$$

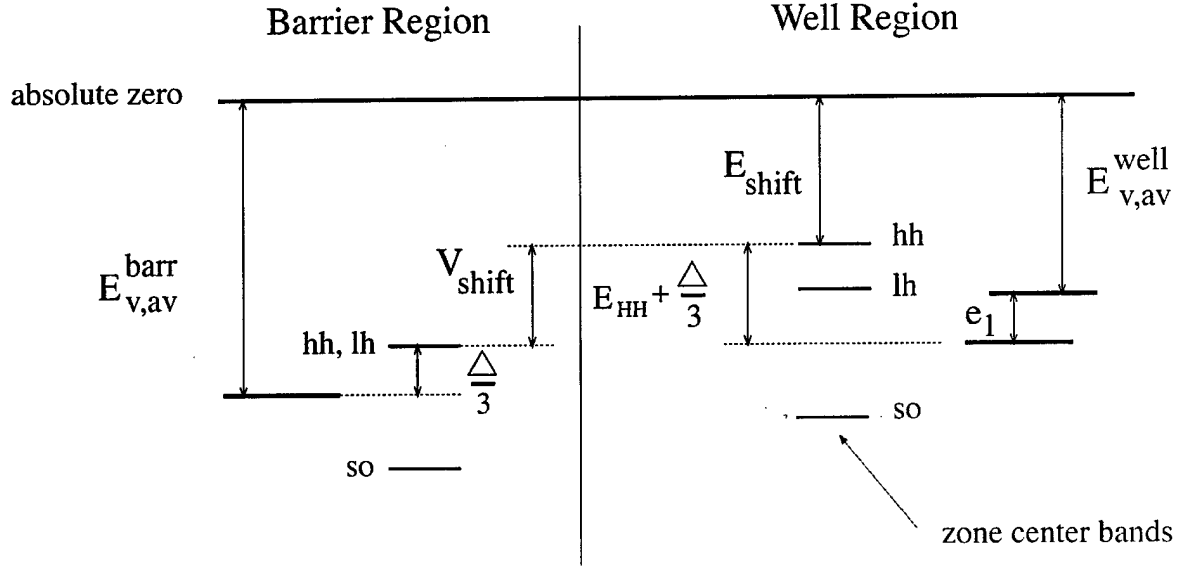


Figure 7 Definition of absolute valence band energy.

The values for V_b and V_w are determined based on the average valence band energies of the well and barrier material. In order to stay consistent with convention, a constant value is included that will shift the zone center ($k = 0$) heavy hole band in the well bulk material to zero. The values for V_b and V_w can be expressed as

$$V_w = E_{v,av}^{well} + \frac{\Delta^{well}}{3} + e_1^{well} \quad (36a)$$

$$V_b = E_{v,av}^{barr} + \frac{\Delta^{barr}}{3} \quad (36b)$$

$$E_{shift} = E_{v,av}^{well} + e_1^{well} + \frac{\Delta^{well}}{3} + E_{HH} \quad (36c)$$

The term E_{HH} comes from the diagonalization of the matrix $H_{so} + H_{strain}$ and represents the shift in the heavy hole band from the unstrained position in the bulk dispersion relations. Again, the objective of subtracting E_{shift} is to bring the zone center energy of the heavy hole band in the bulk dispersion relations of the well material to zero and is done for convention only.

2.2.2.2 k_z as a Function of Energy and k -parallel. Now that the Hamiltonians for both the well and the barrier are well defined for any value of \mathbf{k} , the next step is to invert the expression to a form of k_z as a function of energy E and \mathbf{k}_{\parallel} . This is done through a method presented by Szmulowicz (6).

The total Hamiltonian, given by $H_{k,p} + H_{so} + H_{strain}$ can be factored in terms of k_z where

$$H = H_2 k_z^2 + H_1 k_z + H_0 \quad (37)$$

and H_2 , H_1 , and H_0 are 6x6 matrices that are functions of $\mathbf{k}_{\parallel} = k_x + k_y$. Incorporating this expression of the Hamiltonian into the time-independent Schrodinger equation

$$\hat{H}\psi = E\psi \quad (38)$$

gives the following expression relating k_z , E , H_2 , H_1 , and H_0

$$k_z^2 \psi + H_2^{-1} H_1 k_z \psi + H_2^{-1} (H_0 - E) \psi = 0 \quad (39)$$

Defining a vector ϕ as

$$\phi \equiv k_z \psi \quad (40)$$

and substitution into equation 39 yields

$$k_z \phi + H_2^{-1} H_1 \phi + H_2^{-1} (H_0 - E) \psi = 0 \quad (41a)$$

$$k_z \psi - \phi = 0 \quad (41b)$$

Through algebraic manipulation, the system of equations can be expressed in a matrix equation of the following form

$$\begin{pmatrix} -k_z I & I \\ -H_2^{-1}(H_0 - E) & -H_2^{-1}H_1 - k_z I \end{pmatrix} \begin{pmatrix} \psi \\ k_z \psi \end{pmatrix} = 0 \quad (42)$$

where I is a 6×6 unit matrix. If k_z is considered an eigenvalue, the problem can be considered an eigenvalue problem of the form $(M - \lambda I)\chi = 0$ expressed as

$$\left[\begin{pmatrix} 0 & I \\ -H_2^{-1}(H_0 - E) & -H_2^{-1}H_1 \end{pmatrix} - \begin{pmatrix} k_z I & 0 \\ 0 & k_z I_{6 \times 6} \end{pmatrix} \right] \begin{pmatrix} \psi \\ k_z \psi \end{pmatrix} = \begin{pmatrix} 0 \\ 0 \end{pmatrix} \quad (43)$$

where

$$M = \begin{pmatrix} 0 & I_{6 \times 6} \\ -H_2^{-1}(H_0 - E) & -H_2^{-1}H_1 \end{pmatrix} \quad (44)$$

and

$$\chi = \begin{pmatrix} \psi \\ k_z \psi \end{pmatrix} \quad (45)$$

By finding the eigenvalues of this complex non-Hermitian matrix, k_z can be extracted for any value of energy E . By finding the eigenvectors of the matrix M , the eigenvectors associated with each value of k_z can also be determined. The method used to determine the eigenvectors and eigenvalues are presented in section 3.2.

2.2.2.3 Envelope Functions. Envelope functions are linear combinations of bulk material wavefunctions where the periodic piece of the Bloch function, $u_{n\mathbf{k}=0}(\mathbf{r})$, is not included. The flat-band approximation states that the periodic part of the Bloch functions in the well and the barrier are approximately equal, i.e. $u_{n\mathbf{k}=0}(\mathbf{r})$ is continuous (13). Using this approximation, $u_{n\mathbf{k}=0}(\mathbf{r})$ can be

excluded when imposing boundary conditions. Through symmetry analysis, the envelope functions in the well region and the barrier region can be expressed in matrix notation as

$$F^b(\mathbf{k}_{\parallel}, z) \equiv (\Gamma C^b) E^b(-z) B \quad (46)$$

$$F^w(\mathbf{k}_{\parallel}, z) \equiv [C^w E^w(z) \pm \Gamma C^w E^w(-z)] W \quad (47)$$

where Γ is a reflection operator defined as

$$\Gamma = \begin{pmatrix} 1 & 0 & 0 & 0 & 0 & 0 \\ 0 & -1 & 0 & 0 & 0 & 0 \\ 0 & 0 & 1 & 0 & 0 & 0 \\ 0 & 0 & 0 & -1 & 0 & 0 \\ 0 & 0 & 0 & 0 & -1 & 0 \\ 0 & 0 & 0 & 0 & 0 & 1 \end{pmatrix} \quad (48)$$

and represents a reflection about the origin. This operator is used with the parity of the wave functions to reduce the number of boundary conditions (2).

C is a matrix consisting of the eigenvectors specifying the linear combination of plane waves making up the bulk material wave functions. The matrix C consists of the eigenvectors in column form and is determined by the process described in the previous section. C can be expressed as

$$C = \begin{pmatrix} \psi_{hh} & \psi_{lh} & \psi_{lh} & \psi_{hh} & \psi_{so} & \psi_{so} \end{pmatrix} \quad (49)$$

where ψ_x represent the eigenvectors associated with the eigenvalues of k_z in column form.

The E matrices contain the plane wave portions of the wave functions and utilize the eigenvalues of k_z . They are defined in both directions. For the positive

z direction

$$E^{b,w}(z) = \begin{pmatrix} e^{ik_z^{hh}z} & 0 & 0 & 0 & 0 & 0 \\ 0 & e^{ik_z^{lh}z} & 0 & 0 & 0 & 0 \\ 0 & 0 & e^{ik_z^{lh}z} & 0 & 0 & 0 \\ 0 & 0 & 0 & e^{ik_z^{hh}z} & 0 & 0 \\ 0 & 0 & 0 & 0 & e^{ik_z^{so}z} & 0 \\ 0 & 0 & 0 & 0 & 0 & e^{ik_z^{so}z} \end{pmatrix} \quad (50)$$

and for the negative z direction

$$E^{b,w}(-z) = \begin{pmatrix} e^{-ik_z^{hh}z} & 0 & 0 & 0 & 0 & 0 \\ 0 & e^{-ik_z^{lh}z} & 0 & 0 & 0 & 0 \\ 0 & 0 & e^{-ik_z^{lh}z} & 0 & 0 & 0 \\ 0 & 0 & 0 & e^{-ik_z^{hh}z} & 0 & 0 \\ 0 & 0 & 0 & 0 & e^{-ik_z^{so}z} & 0 \\ 0 & 0 & 0 & 0 & 0 & e^{-ik_z^{so}z} \end{pmatrix} \quad (51)$$

W and B are eigenvectors that specify the linear combination of bulk material wavefunctions that make up the envelope functions in the well and barrier respectively.

2.2.2.4 Boundary Conditions. The boundary conditions are similar to those required in the one-dimensional square well problem. For the simple square well problem the boundary conditions require: (1) the wave functions are continuous at the well/barrier boundaries, (2) the derivatives of the wave functions are continuous at the well/barrier boundaries, and (3) the wave functions approach zero at $\pm\infty$. These wave functions and their derivatives must be continuous in order to correspond to an observable probability density. If the derivatives were not continuous the presence of a singular potential would be implied. Finally, the

wave functions must be finite everywhere and square integrable which requires the wave functions to approach zero at $\pm\infty$ (14).

The requirements for the semiconductor quantum well are essentially the same as those stated above. For bound carriers, the wavefunctions must decay exponentially in the barrier to ensure the wave functions remain finite everywhere. The wave functions must also be continuous at the heterostructures as before. However, due to the differences in bandstructure in the barrier and the well materials, the effective masses will change at the barrier/well interface. For a simple 1D quantum well this results in the boundary condition for the derivative to be

$$\frac{1}{m^b} \frac{\partial}{\partial z} F^b = \frac{1}{m^w} \frac{\partial}{\partial z} F^w \quad (52)$$

Through the use of the definition of the effective mass and the expression of the total Hamiltonian factored with respect to k_z , the boundary conditions using the 6×6 $k \cdot p$ bulk eigenfunctions can be expressed as (2)

$$F^b = F^w \quad (53)$$

$$H_2^b \frac{\partial}{\partial z} F^b + \frac{H_1^b}{-2i} F^b = H_2^w \frac{\partial}{\partial z} F^w + \frac{H_1^w}{-2i} F^w \quad (54)$$

where F^b and F^w are the envelope functions in the barrier and the well and H_2 and H_1 are from equation 37.

Using the boundary conditions stated in equations 53 and 54 and the form of the envelope functions in equations 46 and 47, a matrix equation can be expressed as

$$\begin{pmatrix} M^w & -M^b \\ H_2^w N^w + \frac{H_1^w}{2} M^w & -(H_2^b N^b + \frac{H_1^b}{2} M^b) \end{pmatrix} \begin{pmatrix} W \\ B \end{pmatrix} = \begin{pmatrix} 0 \\ 0 \end{pmatrix} \quad (55)$$

where the values of M^w , M^b , N^w , N^b are defined as

$$M^w = C^w E^w(z) + \Gamma C^w E^w(-z) \quad (56a)$$

$$M^b = C^b E^b(z) \quad (56b)$$

$$N^w = C^w K^w E^w(-z) - \Gamma C^w K^w E^w(z) \quad (56c)$$

$$N^b = C^b K^b E^b(z) \quad (56d)$$

The matrices C , Γ , $E(-z)$, and $E(+z)$ were defined in section 2.2.2.2

The K matrices consist of the eigenvalues for $k_z = k_z(E)$ found earlier from the eigenvalues of equation 44 and are arranged as follows for both the well and barrier

$$K^{b,w} = \begin{pmatrix} k_z^{hh} & 0 & 0 & 0 & 0 & 0 \\ 0 & k_z^{lh} & 0 & 0 & 0 & 0 \\ 0 & 0 & k_z^{lh} & 0 & 0 & 0 \\ 0 & 0 & 0 & k_z^{hh} & 0 & 0 \\ 0 & 0 & 0 & 0 & k_z^{so} & 0 \\ 0 & 0 & 0 & 0 & 0 & k_z^{so} \end{pmatrix} \quad (57)$$

where hh , lh , and so correspond to the heavy hole, light hole, and split off bands.

2.2.3 Quantum Well Dispersion Relationships. As was done for the simple quantum well problem, the matrix equation describing the boundary conditions given in equation 55 can be assumed to be an eigenvalue problem, with an eigenvalue equal to zero. Therefore, the boundary conditions can only be satisfied if the determinant of the matrix in equation 55 is equal to zero. The methods used to compute the matrices described in this section and ultimately find the determinant of the boundary conditions matrix as a function of energy E are described in the following chapter.

III. Computational Approach

This chapter explains the approach taken in calculating dispersion curves for both bulk material and quantum wells. Also discussed is the development of the computational tools necessary to perform the specific calculations.

3.1 Bulk Material Calculations

The bulk material band structure requires determining the eigenvalues of a 6×6 complex Hermitian matrix. The total Hamiltonian matrix consists of the $\mathbf{k} \cdot \mathbf{p}$ Hamiltonian, the spin-orbit Hamiltonian, and the strain Hamiltonian. The system must be solved for every value of the inverse wave vector \mathbf{k} . This is accomplished through the use of standard eigenvalue subroutines discussed in section 3.3.

3.2 Quantum Well Calculations

Developing the quantum well dispersion curves first requires determination of the zone center energies for each band. This is accomplished through thorough analysis of the function relating the determinant of the boundary condition matrix to energy. Each root of this complex function identifies a quantum well energy band at a particular value of \mathbf{k}_{\parallel} . These values are then utilized as initial guesses in a root-finding algorithm that determines roots of the function for each incremental step in \mathbf{k}_{\parallel} .

The two significant steps involved in the quantum well problem are the expression of k_z as function of energy E and then finding the determinant of the matrix describing the quantum well boundary conditions. Both steps are explained in the following sections.

3.2.1 Eigenvalues and Eigenvectors of $k_z(E)$. The total Hamiltonian is first presented in the factored form. Recall from section 2.2.2.2 that the Hamil-

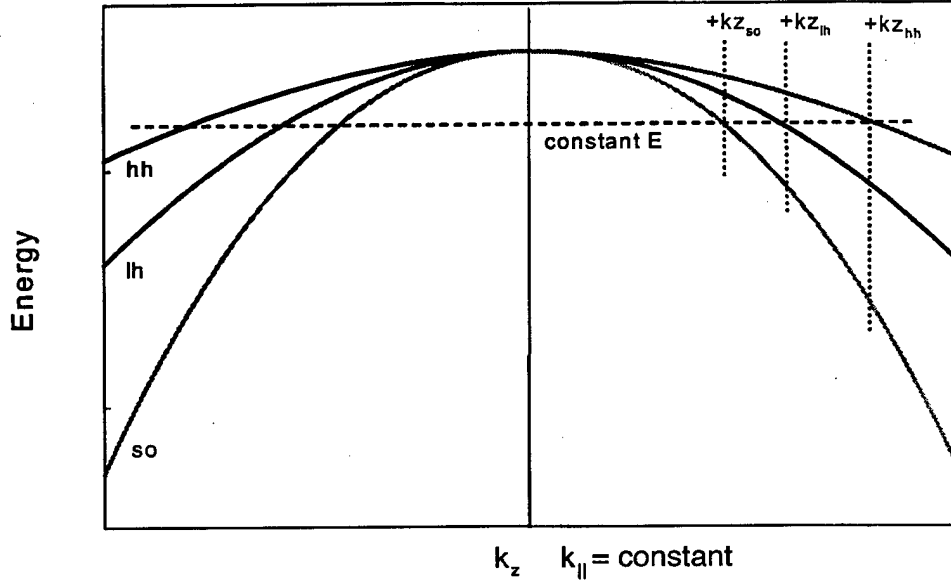


Figure 8 Schematic of a bulk dispersion curve showing energy as a function of k_z and k_z as a function of energy (2).

tonian is factored in powers of k_z to yield $H_{total} = H_2 k_z^2 + H_1 k_z + H_0$. The coefficients of the factored Hamiltonian are then utilized to develop the matrix equation describing the inverse wave vector component $k_z = k_z(E, \mathbf{k}_{||})$ as a function of energy and $\mathbf{k}_{||}$. The complete set of 12 eigenvalues and eigenvectors for this system consist of only 6 linearly independent vectors and 6 doubly degenerate eigenvalues. Therefore, selection of the correct eigenvalues and the corresponding eigenvectors is necessary.

If X is the transformation matrix used to diagonalize the matrix in equation 43, it consists of the system's eigenvectors in column form and can be expressed as

$$X = \begin{pmatrix} X_{11} & X_{12} \\ X_{21} & X_{22} \end{pmatrix} \quad (58)$$

The column vectors in X_{21} and X_{22} will be equal to the X_{11} and X_{12} multiplied by the associated eigenvalue. This is apparent through the expression given in equation 42. As shown in figure 8, for every positive value of k_z there exists

a corresponding negative value. The eigenvectors associated with the negative eigenvalues can be shown to be equal to the vectors associated with the positive eigenvalues with the exception of a phase factor. Thus, all positive eigenvalues and associated eigenvectors are selected and the rest excluded from further calculations. It must also be noted that k_z will become pure imaginary when the value of energy is greater than the maximum energy of the associated band. In this case, there is still a negative pure imaginary eigenvalue associated with every positive imaginary value. The linear dependence on the eigenvectors hold, so only the positive imaginary values and associated eigenvectors are utilized.

A subroutine must select all positive, pure real and pure imaginary, eigenvalues and associated eigenvectors. It is also important that for each iteration the list of eigenvalues and eigenvectors must be ordered the same way before being passed to the following subroutine for construction of the quantum well boundary condition matrix. The form of the matrices is given below.

$$eigenvalues = \begin{pmatrix} hh \\ lh \\ lh \\ hh \\ so \\ so \end{pmatrix} \quad (59)$$

and for the matrix of eigenvectors C

$$C = \begin{pmatrix} \psi_{hh} & \psi_{lh} & \psi_{lh} & \psi_{hh} & \psi_{so} & \psi_{so} \end{pmatrix} \quad (60)$$

where ψ_x represent the eigenvectors in column form.

In the simplest case, $\mathbf{k}_{\parallel} = 0$, the bulk dispersion curves behave as described above and as shown in figure 8. In this case, the identification of hh , lh , and so

eigenvalues is easily accomplished. However, as k_{\parallel} increases, choosing the correct eigenvalues becomes more complicated because the imaginary values of k_z are much less predictable. Also, as k_{\parallel} increases the bands become double valued as a function of energy. In this case, an algorithm is forced to choose only one of the two valid solutions and assign the second value erroneously to another band. This situation occurs whenever any one of the bands has a maximum not at $k_{\parallel} = 0$. The difficulties in assigning eigenvalues to a specific band can be seen in figures 9 thru 11 which show the bandstructure determined from the $k_z(E)$ inversion process.

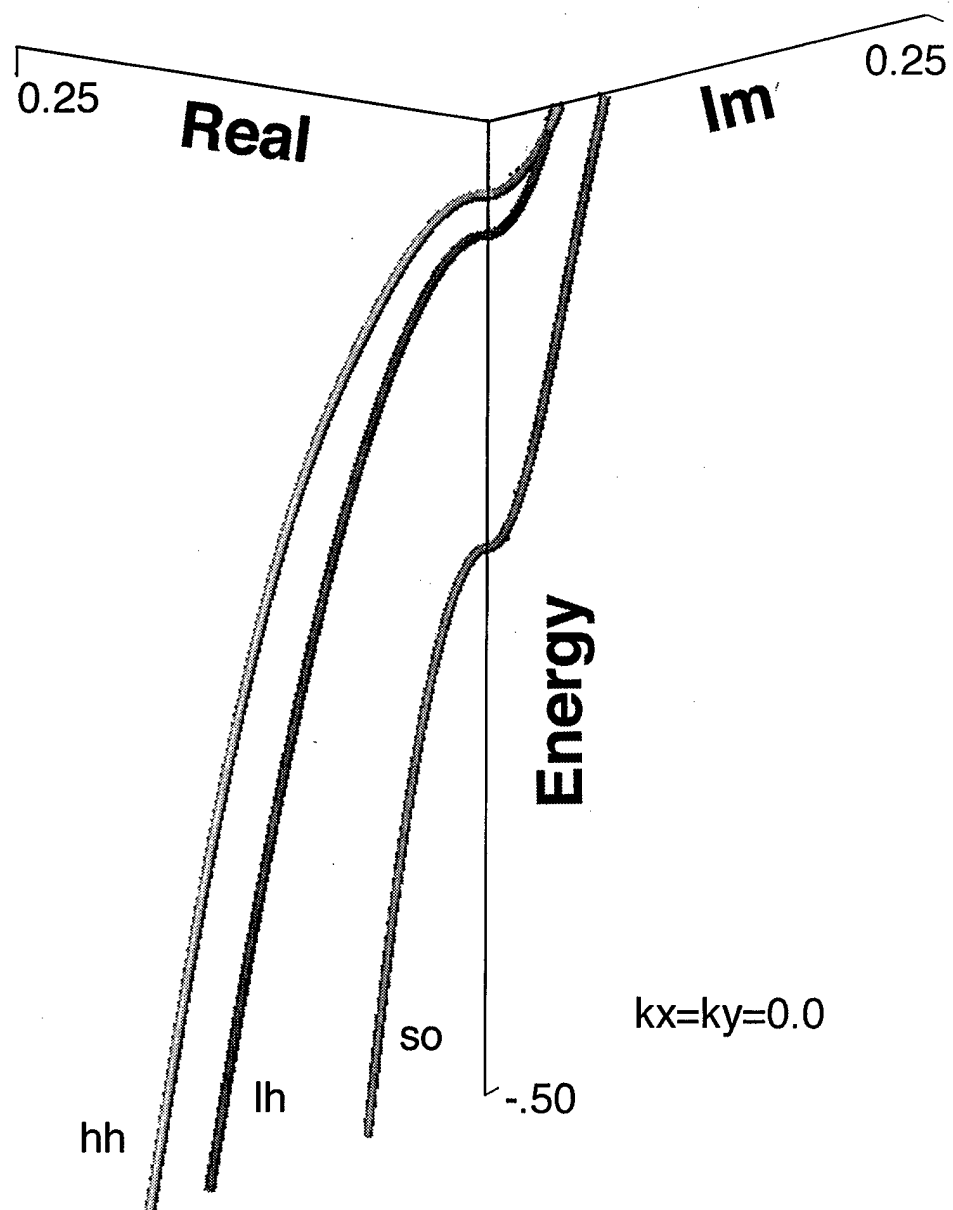


Figure 9 Positive real and positive imaginary values of kz for the lh , hh , and so bands.

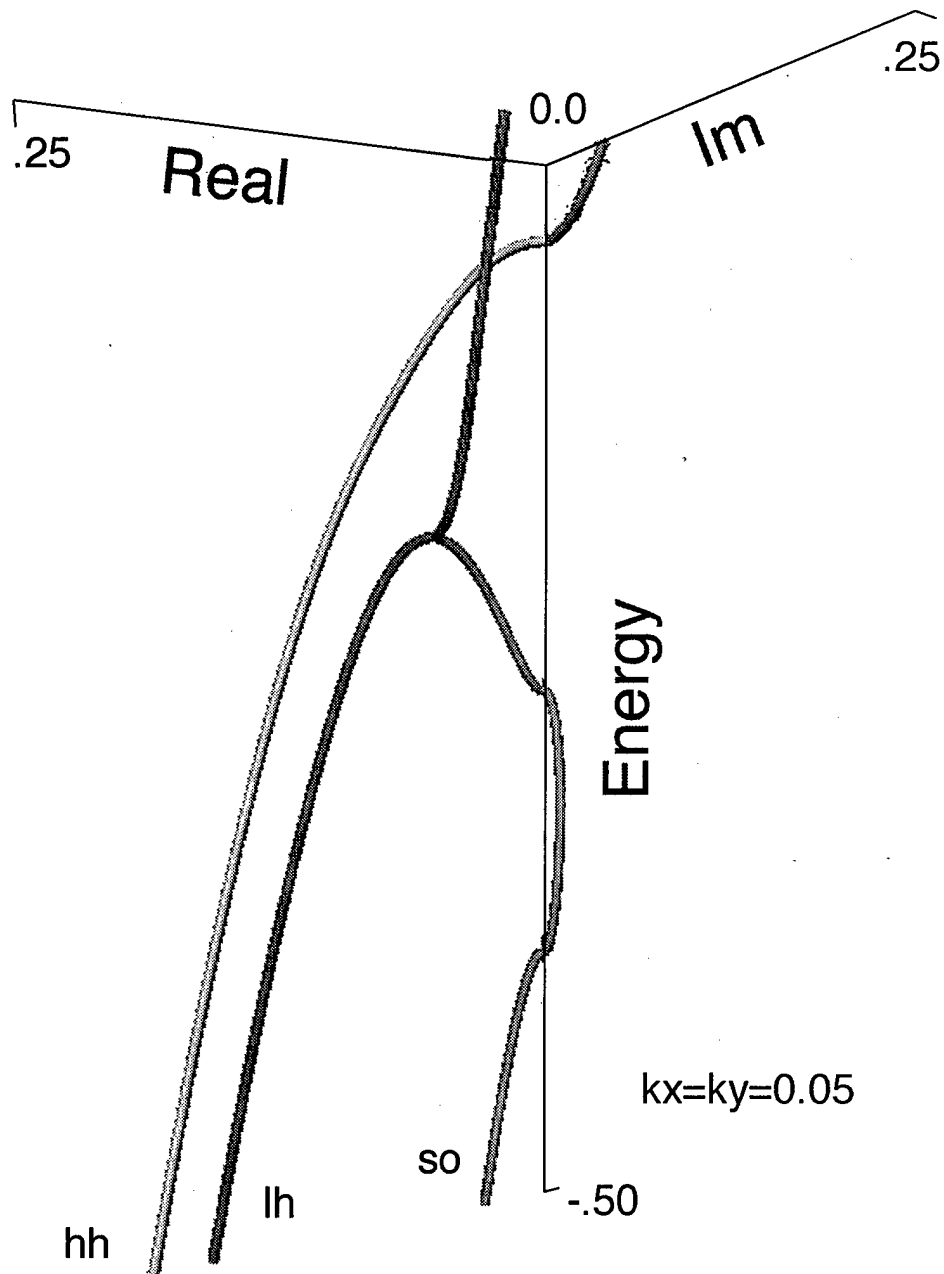


Figure 10 Positive real and positive imaginary values of kz for the lh , hh , and so bands. Note the joining of the lh and so bands at the point corresponding to the maximum energy in the lh band.

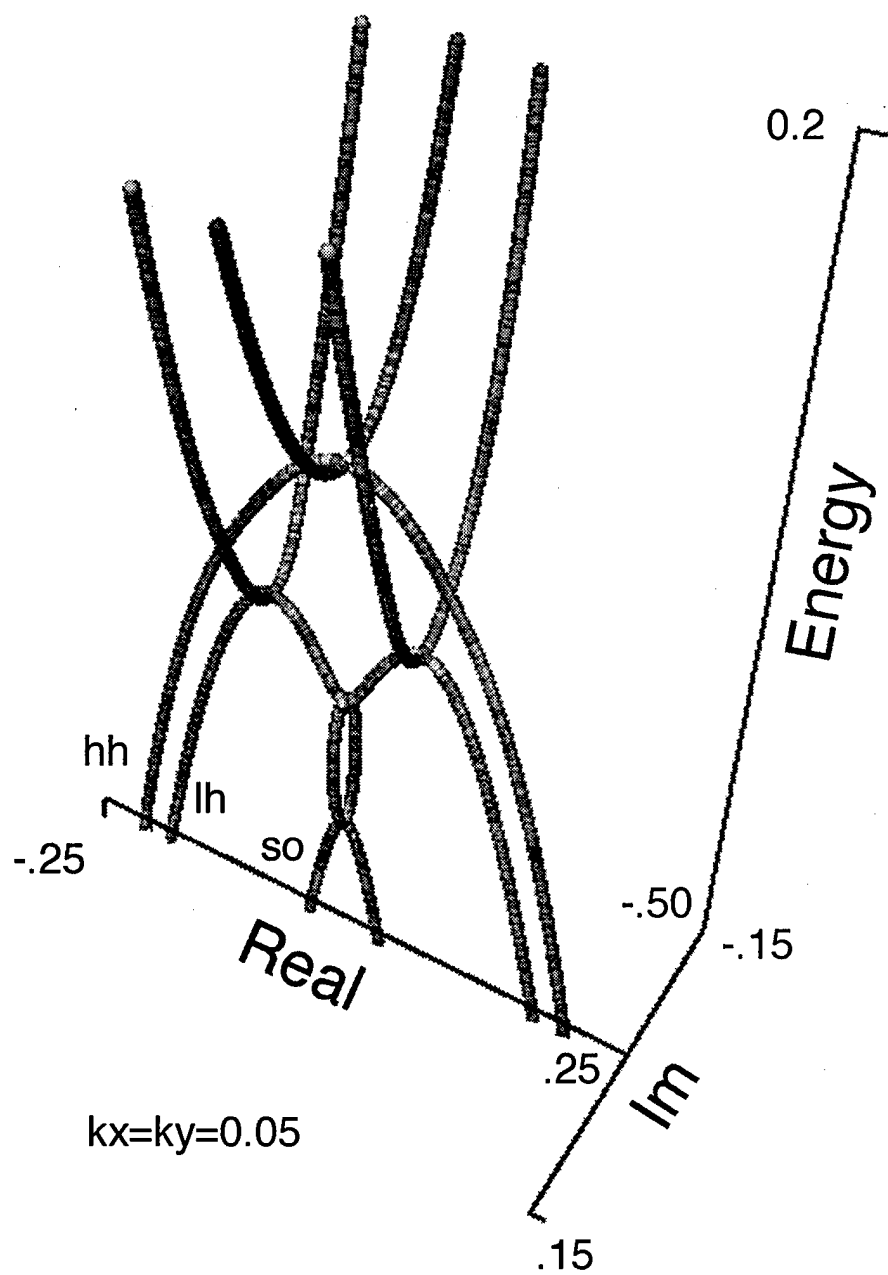


Figure 11 All eigenvalues of the matrix describing k_z as a function of energy.

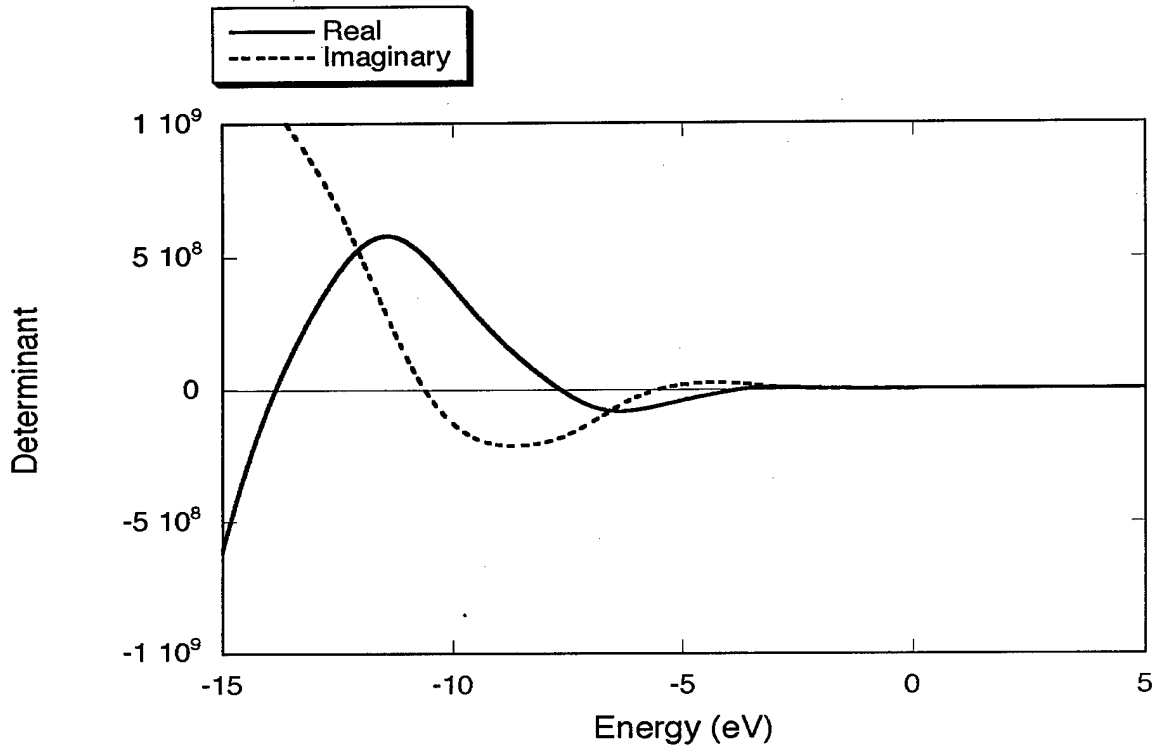


Figure 12 Plot of the determinant of the 30Å Si/SiGe quantum well boundary condition matrix vs. energy. $k_x=k_y=0$.

3.2.2 Determinant of Boundary Condition Matrix. Once the appropriate eigenvalues and associated eigenvectors for k_z are determined the matrix equation describing the boundary conditions for the quantum well is generated. As shown in section 2.2.3, an acceptable value of energy is found for a particular value of $k_{||}$ when the determinant of the matrix in equation 55 is equal to zero.

An analysis of a plot of the real and imaginary values of the determinant of the aforementioned matrix will allow identification of the roots of the function for a particular value of $k_{||}$. Examples of these plots are shown in figures 12 and 13. Figure 12 shows a wide range of values for energy but closer analysis shows that roots only exist in the small region corresponding to the well. An enhanced plot of the data for the region of the well is shown in figure 12.

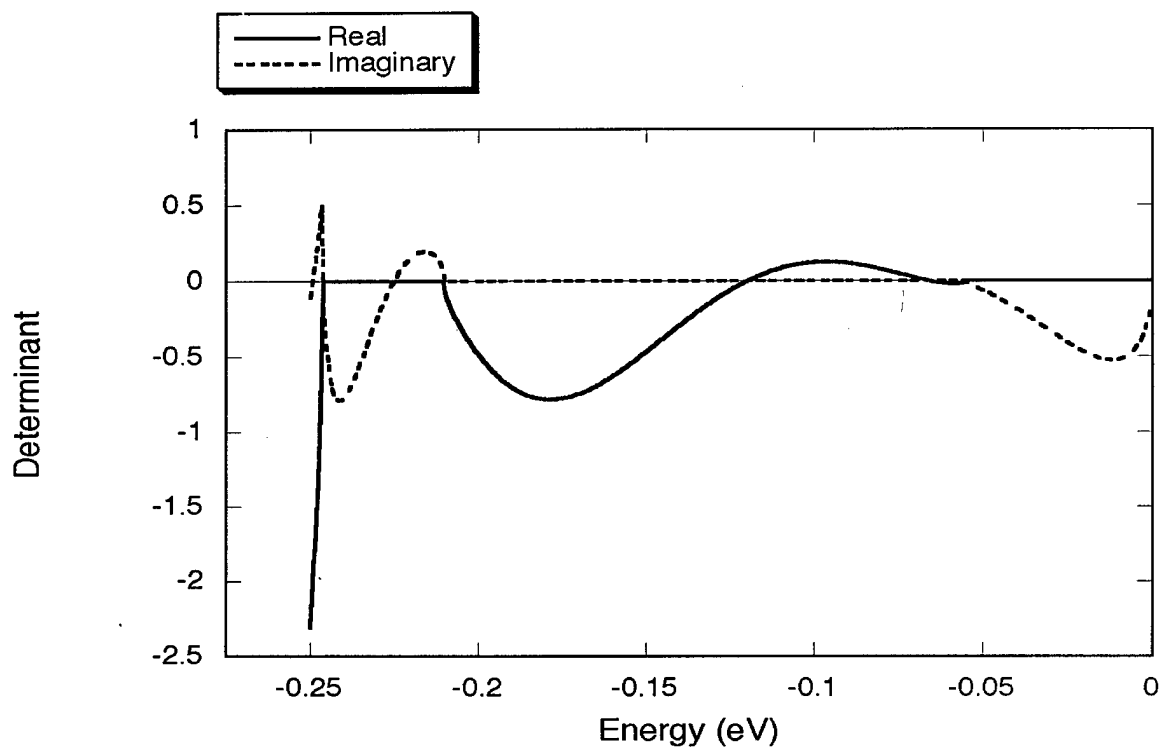


Figure 13 Plot of the determinant of the 30Å Si/SiGe quantum well boundary condition matrix vs. energy. $k_x=k_y=0$.

Using these roots as seed values, the process is repeated at increasing values of k_{\parallel} with a root finder. k_{\parallel} is incrementally increased in a particular direction in the plane of the quantum well to determine the zeros at that new value of k_{\parallel} . These values are then used as the new seed values for the next iteration.

Since the initial roots at $k_{\parallel} = 0$ were determined with good accuracy in the first step of the problem analysis, a modified secant method is acceptable when finding roots at higher values of k_{\parallel} . The secant method is a modification of Newton's method and is shown graphically in figure 14.

The basic equation governing the secant method is

$$x_2 = x_1 - f(x_1) \frac{x_1 - x_0}{f(x_1) - f(x_0)} \quad (61)$$

Enhancements were made to the basic algorithm to handle difficult roots such as those shown in figures 15 and 16. In many cases such as that shown in figure 15 the real part of the complex function or the imaginary part of the function can be approximately zero. The root finder must determine the best choice, either the real part or the imaginary part of the function, to utilize in the calculation given in the equation above. This is accomplished by comparing the values of the determinant in the vicinity of the seed values. The absolute values of the real and imaginary part are compared. If one is approximately zero within a tolerance, the other is used for the calculation.

In other cases, such as that shown in figure 16, the function approaches zero but never crosses the axis. This sort of false root will cause the root-finder to fail to converge in the specified number of maximum iterations. This problem is avoided through the use of accurate initial values. However, the false root may approach the legitimate root over the course of the calculations. In some cases, the false root may even cross over the legitimate root. This is remedied by ensuring that the root finder will fail to converge in the maximum number of iterations only for the

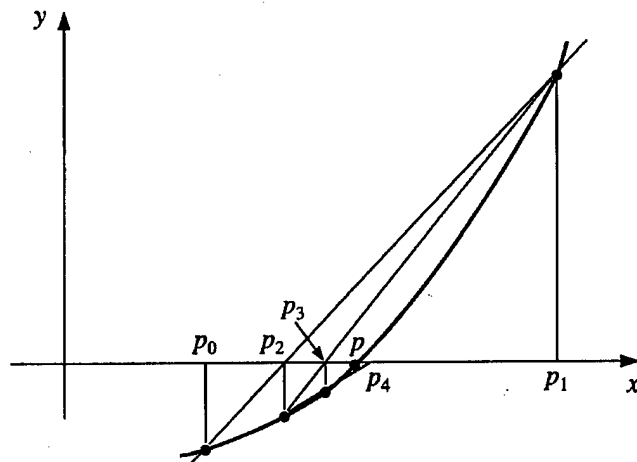


Figure 14 Graphical depiction of the secant method (21).

case of false roots. If the maximum number of iterations is reached, a false root is assumed and a new starting value will be chosen based on the trend of the last two roots found for that particular band. This jump bypasses the false root and facilitate convergence on the legitimate root.

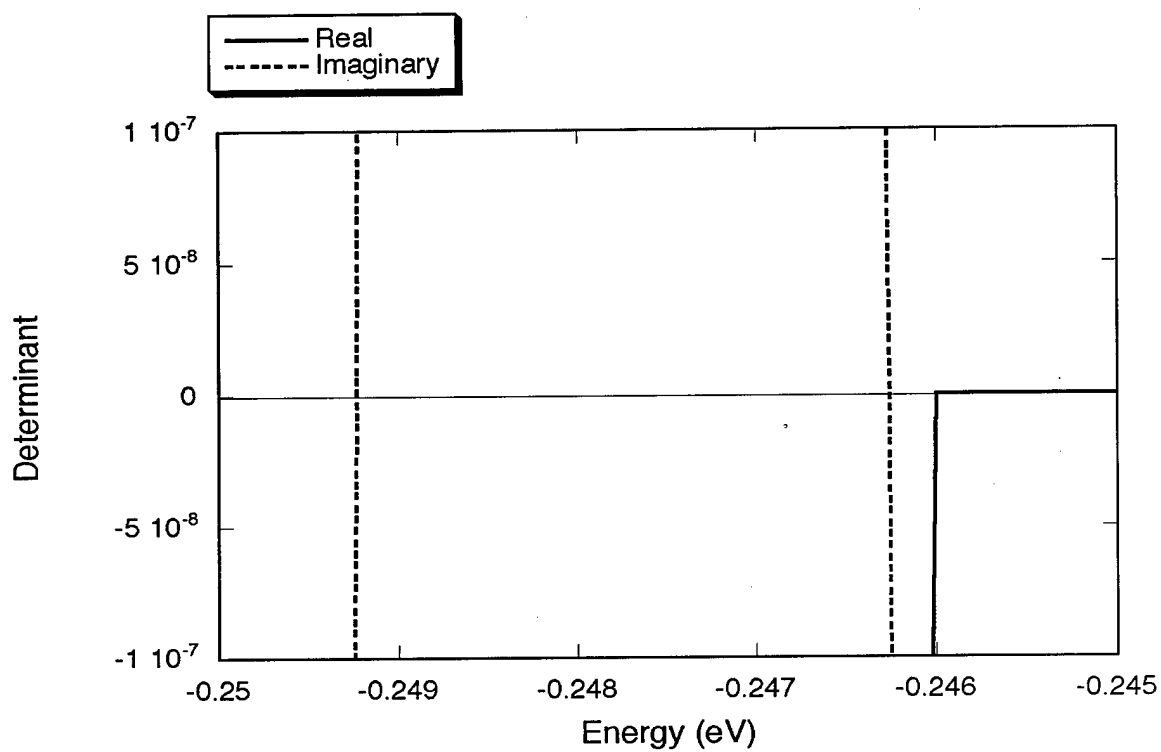


Figure 15 Plot of the determinant of the 30Å Si/SiGe quantum well boundary condition matrix vs. energy.

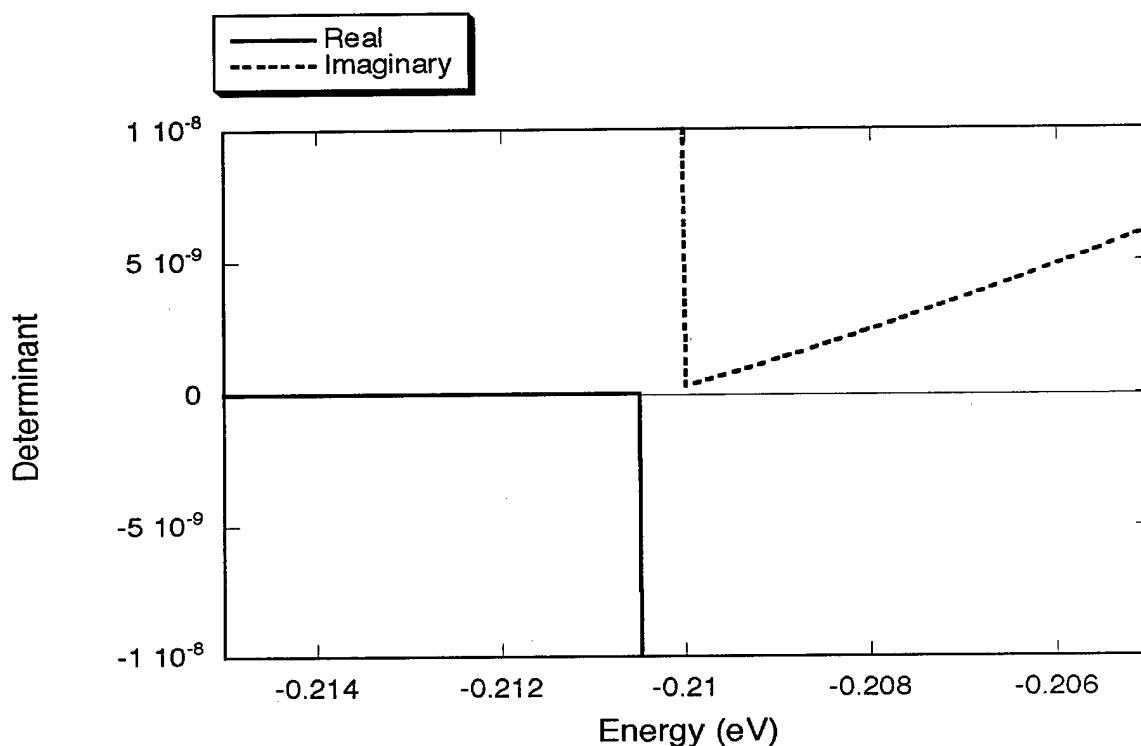


Figure 16 Plot of the determinant of the 30Å Si/SiGe quantum well boundary condition matrix vs. energy.

3.3 Code Generation

The computational tools used in this research were developed in FORTRAN 77. Several linear algebra tools were required to perform tasks such as determining the eigenvalues and eigenvectors of complex non-Hermitian matrices. Several options available were Eigenvalue Subroutine Package (EISPACK), Linear algebra Package (LINPACK), and Linear Algebra Package (LAPACK). LAPACK was chosen as it was the most modern and the most recently updated of the available subroutines.

A software package was developed to compute bandstructures for bulk material and semiconductor quantum wells. The package consists of six programs titled *EFA110*, *EFA001*, *DISP110*, *DISP001*, *BANDS001*, and *BANDS110*.

BANDS001, and *BANDS110* compute strained bulk material band structures for the [110] and [001] growth directions respectively. *EFA110* and *EFA001* compute the determinant of the quantum well boundary condition matrix as a function of energy for any single value of k_{\parallel} . *DISP110* and *DISP001* utilize seed values from *EFA110* and *EFA001* to determine the bandstructure for any azimuthal direction in the plane of the quantum well. All programs and subroutines developed are listed in Appendix A with a brief description of each.

IV. Results and Conclusions

This chapter presents the bulk material band structure and the quantum well bandstructure for several materials. For the quantum wells, both the [110] and the [001] growth directions are evaluated.

4.1 Bulk Material Band Structures

The band structure for alloys consisting of strained Si/Si₇₀Ge₃₀, GaAs, and In₃₀Ga₇₀As are plotted from data files generated using the code described in the previous chapter. Bands for several directions in k -space are evaluated. The zone boundary for these materials is approximately $0.5 \text{ Angstrom}^{-1}$ as given by $\frac{\pi}{a}$ where a is the material's lattice constant.

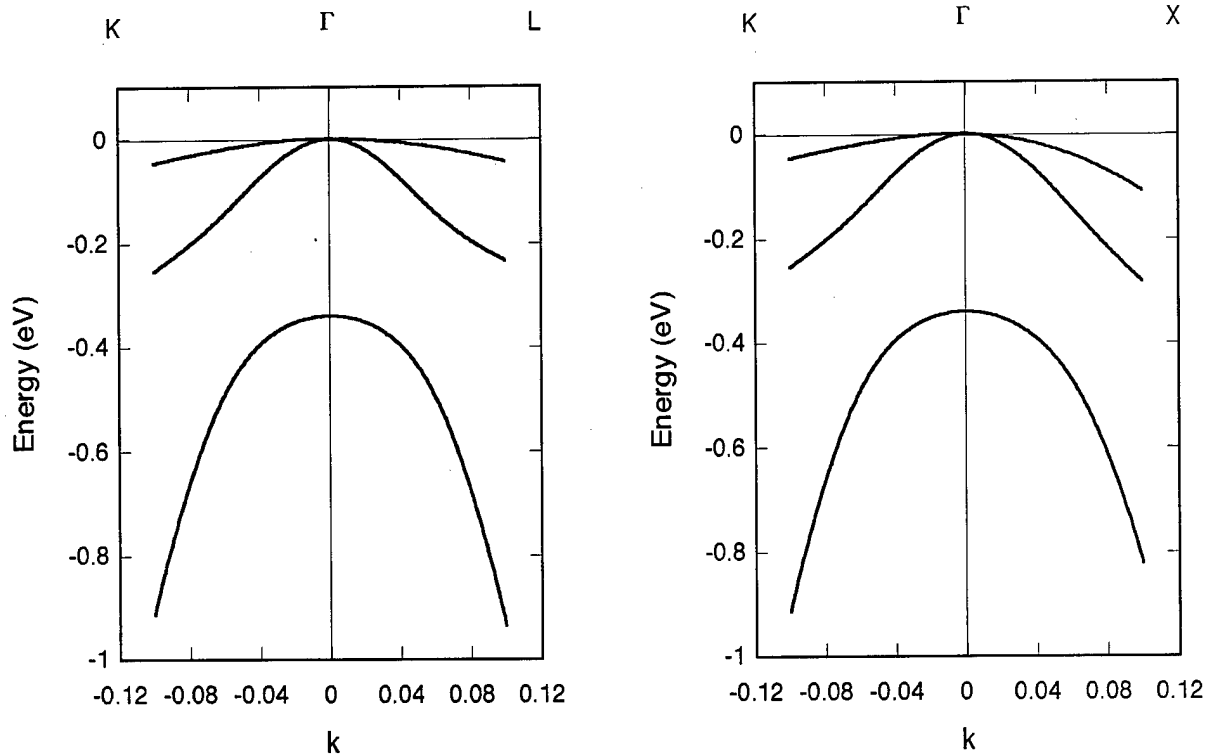


Figure 17 Bulk material dispersion curves for [001] strained GaAs.

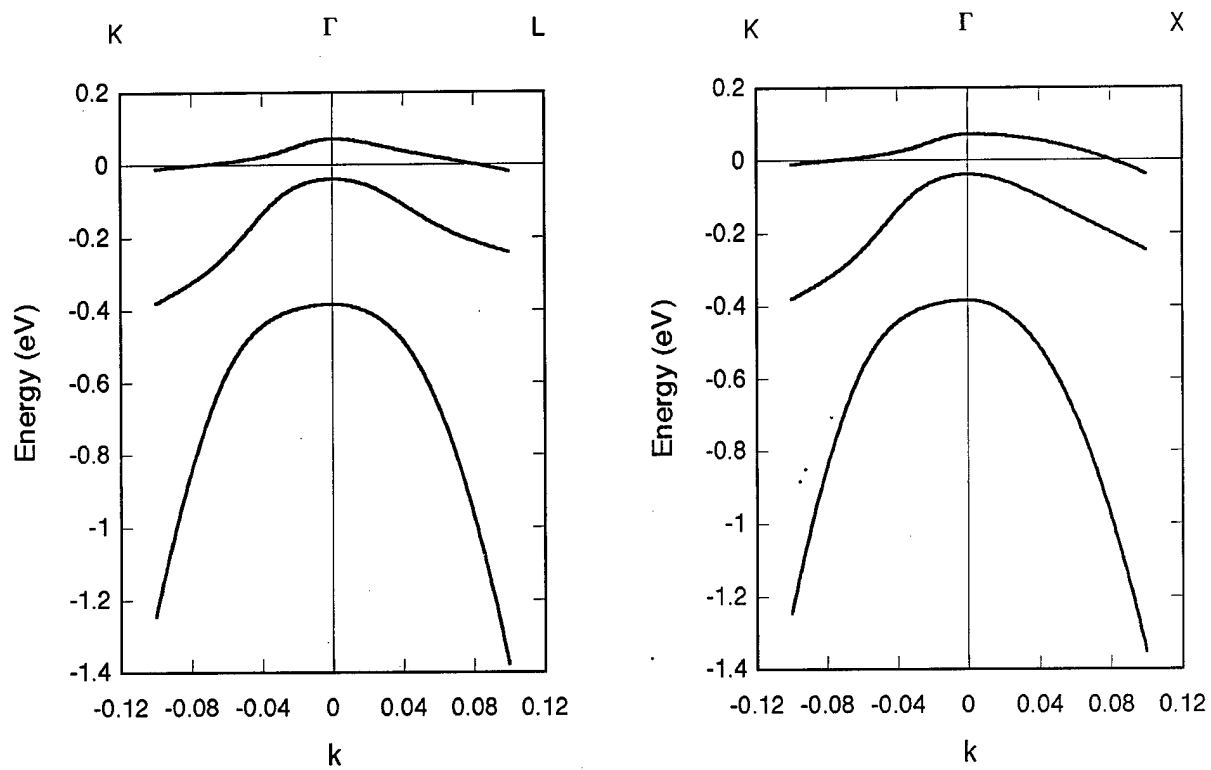


Figure 18 Bulk material dispersion curves for [001] strained $\text{In}_{30}\text{Ga}_{70}\text{As}$.

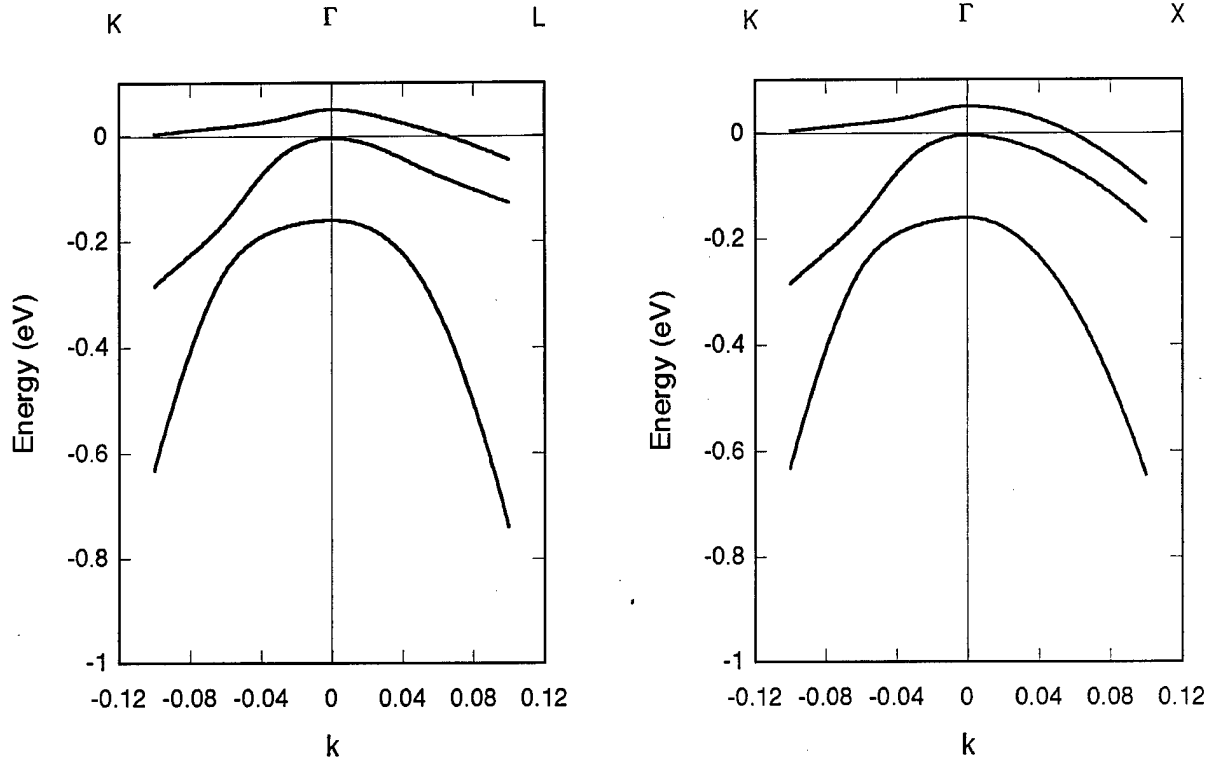


Figure 19 Bulk material dispersion curves for [001] strained $\text{Si}_{70}\text{Ge}_{30}$.

4.2 Quantum Well Band Structures

The band structure for several types of quantum wells are shown for $\text{Si}/\text{Si}_{70}\text{Ge}_{30}$, $\text{Al}_{30}\text{Ga}_{70}\text{As}/\text{GaAs}$, and $\text{GaAs}/\text{In}_{30}\text{Ga}_{70}\text{As}$. The following plots show the evolution of the bandstructure under an azimuthal rotation in k -space. By noticing the evolution of the band structure as the azimuthal angle progresses, the magnitude of the anisotropy can be observed. The directions are defined with respect to the z axis which corresponds to the growth direction. \mathbf{k}_{\parallel} has the components

$$k_x = |\mathbf{k}_{\parallel}| \cos \theta$$

$$k_y = |\mathbf{k}_{\parallel}| \sin \theta$$

The band structures in the following plots are shown as a function of the azimuthal angle θ . The final plots show surfaces representing the bandstructure in the positive k_x and k_y quadrant.

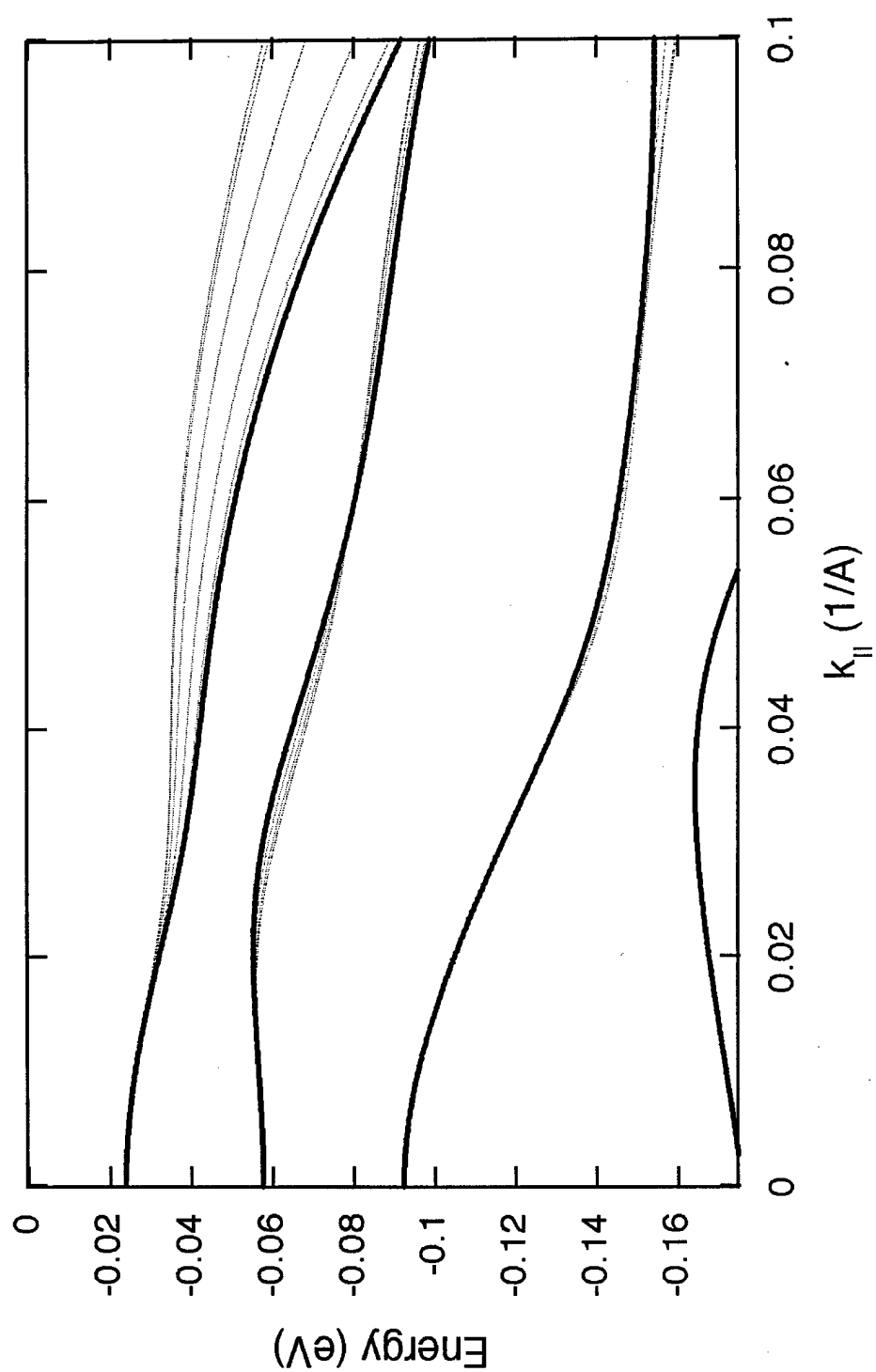


Figure 20 Dispersion curves for [001] $\text{Al}_{30}\text{Ga}_{70}\text{As}/\text{GaAs}$ quantum well with $L=50$ angstrom. Theta ranges from 0 (dark line) to 45 degrees in 10 degree increments (dashed lines).

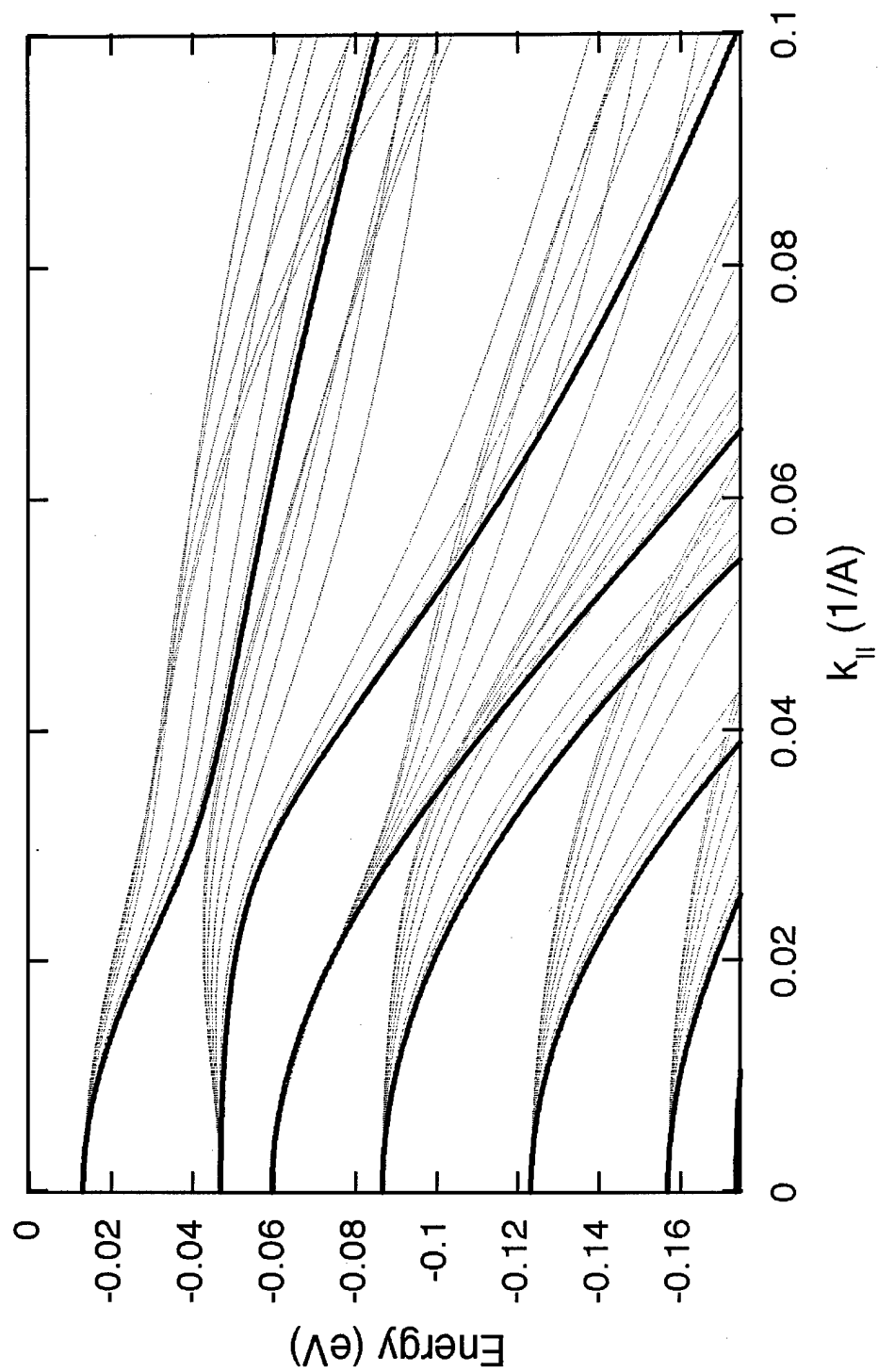


Figure 21 Dispersion curves for [110] $\text{Al}_{30}\text{Ga}_{70}\text{As}/\text{GaAs}$ quantum well with $L=50$ angstrom. Theta ranges from 0 (dark lines) to 90 degrees in 10 degree increments (dashed lines).

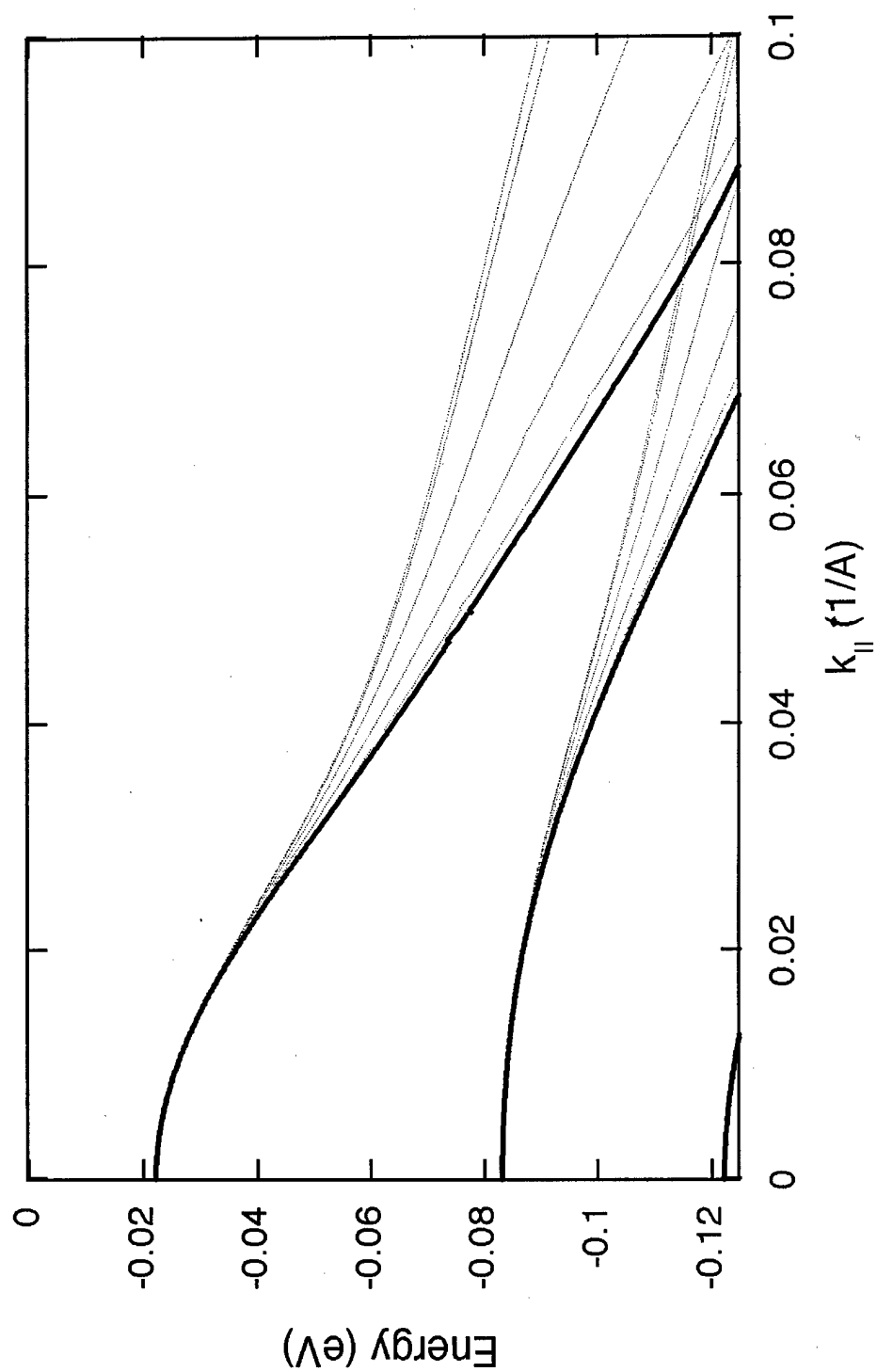


Figure 22 Dispersion curves for [001] $\text{In}_{30}\text{Ga}_{70}\text{As}/\text{GaAs}$ quantum well with $L=50$ angstrom. Theta ranges from 0 (dark line) to 45 degrees in 10 degree increments (dashed lines).

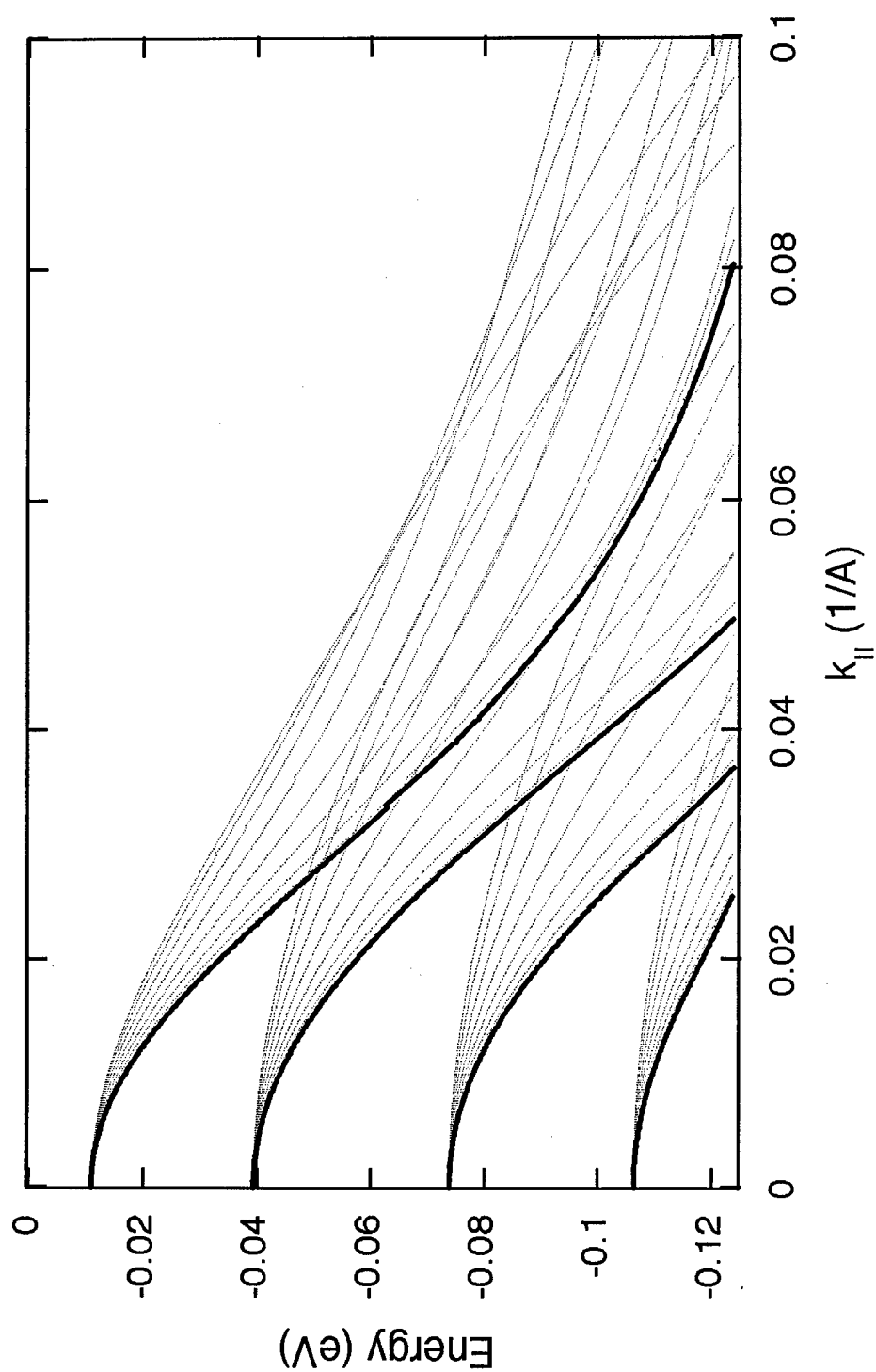


Figure 23 Dispersion curves for [110] $\text{In}_{30}\text{Ga}_{70}\text{As}/\text{GaAs}$ quantum well with $L=50$ angstrom. Theta ranges from 0 (dark line) to 90 degrees in 10 degree increments (dashed lines).

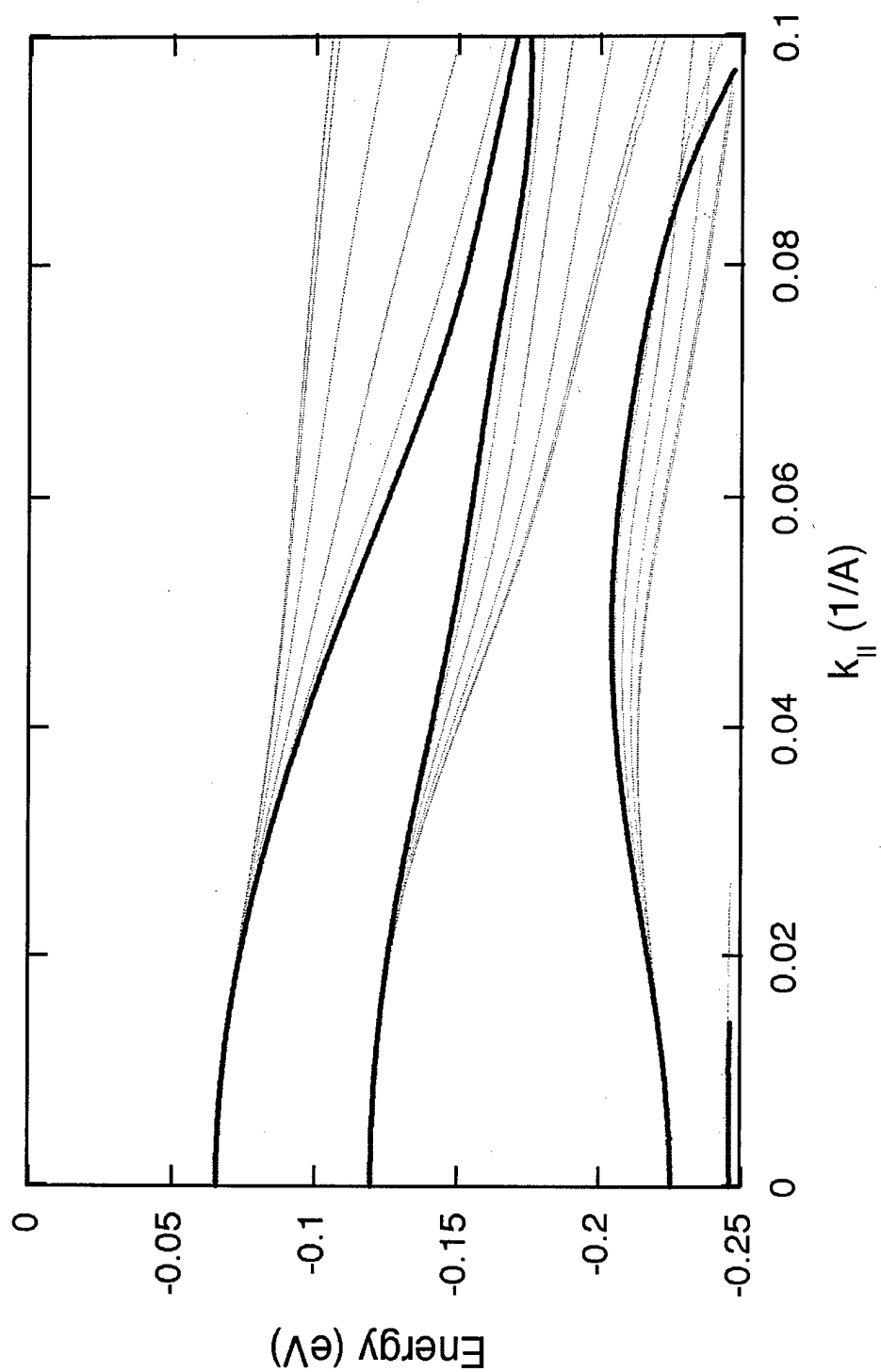


Figure 24 Dispersion curves for [001] Si/Si₇₀Ge₃₀ quantum well with L=30 angstrom. Theta ranges from 0 (dark line) to 45 degrees in 10 degree increments (dashed lines).

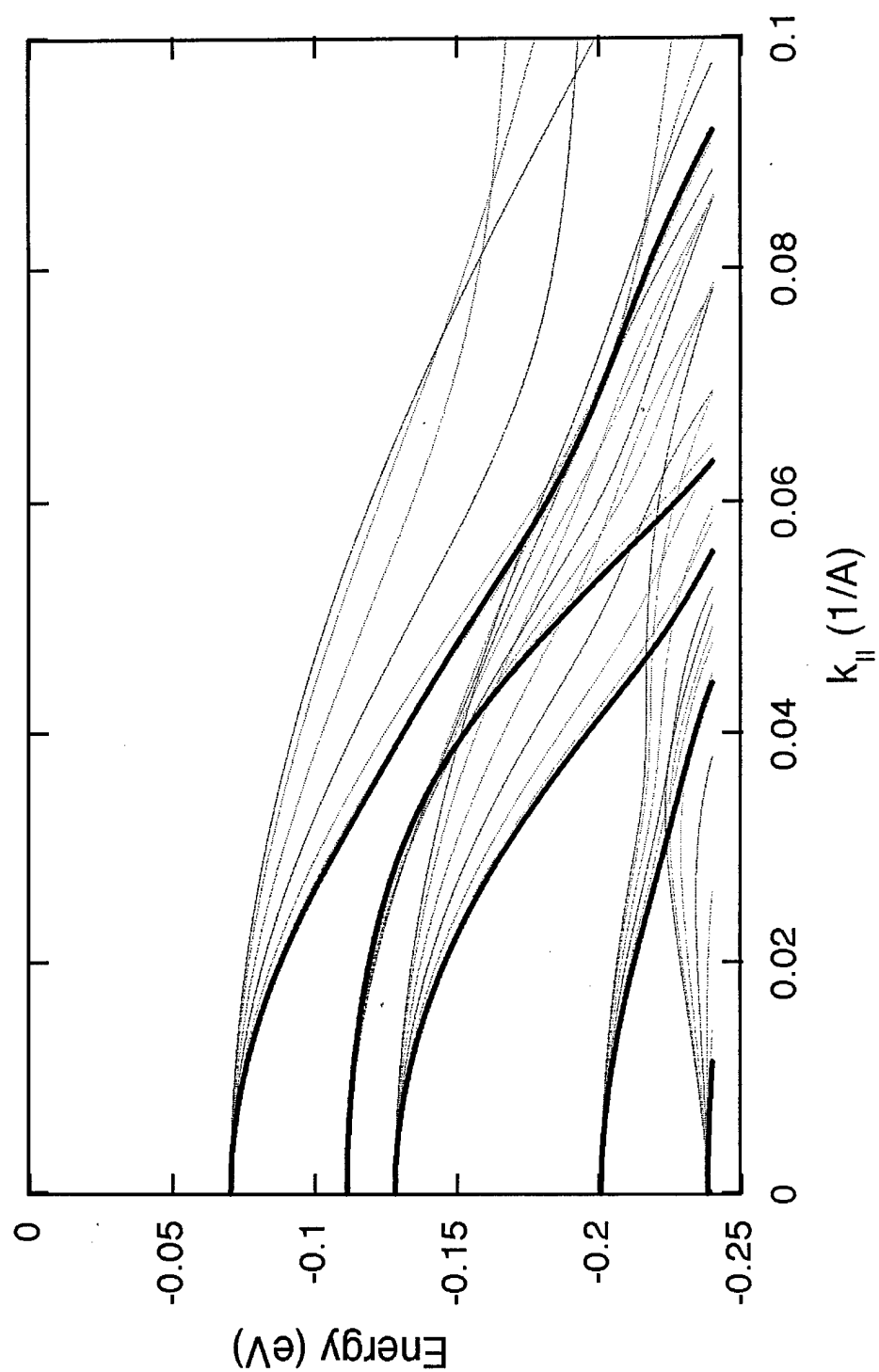


Figure 25 Dispersion curves for [110] Si/Si₇₀Ge₃₀ quantum well with L=30 angstrom. Theta ranges from 0 (dark line) to 90 degrees in 10 degree increments (dashed lines).

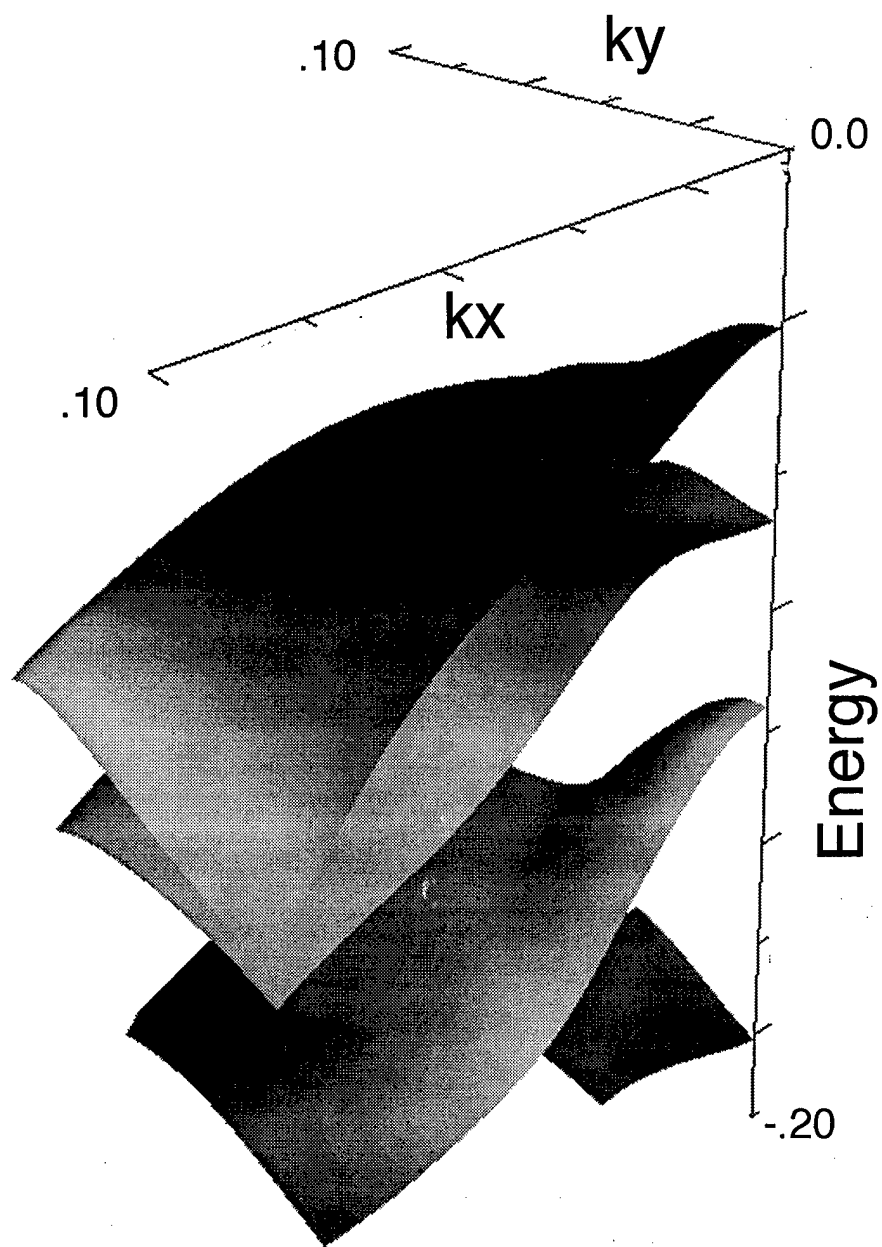


Figure 26 Surface plot of the bandstructure for [001] $\text{Al}_{30}\text{Ga}_{70}\text{As}/\text{GaAs}$ quantum well with $L=50$ angstrom.

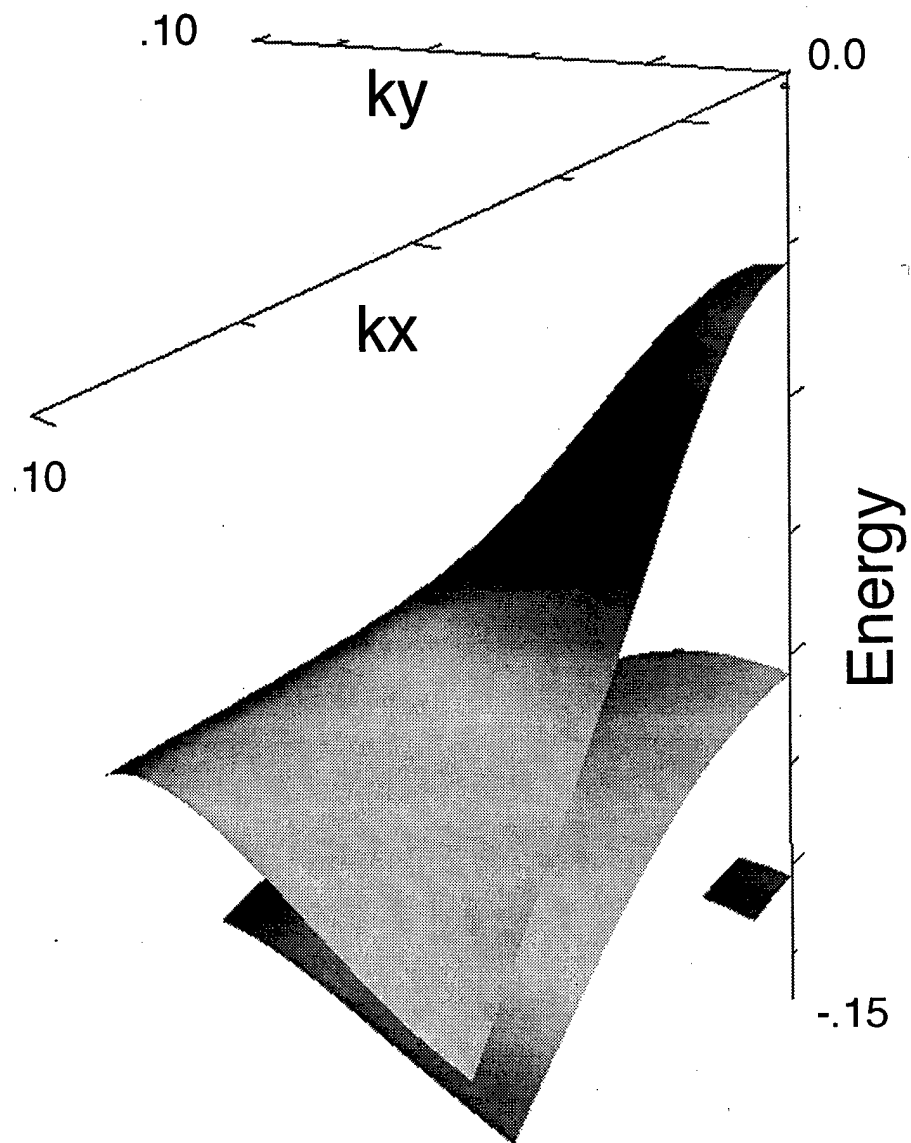


Figure 27 Surface plot of the bandstructure for [001] GaAs/In₃₀Ga₇₀As quantum well with L=50 angstrom.

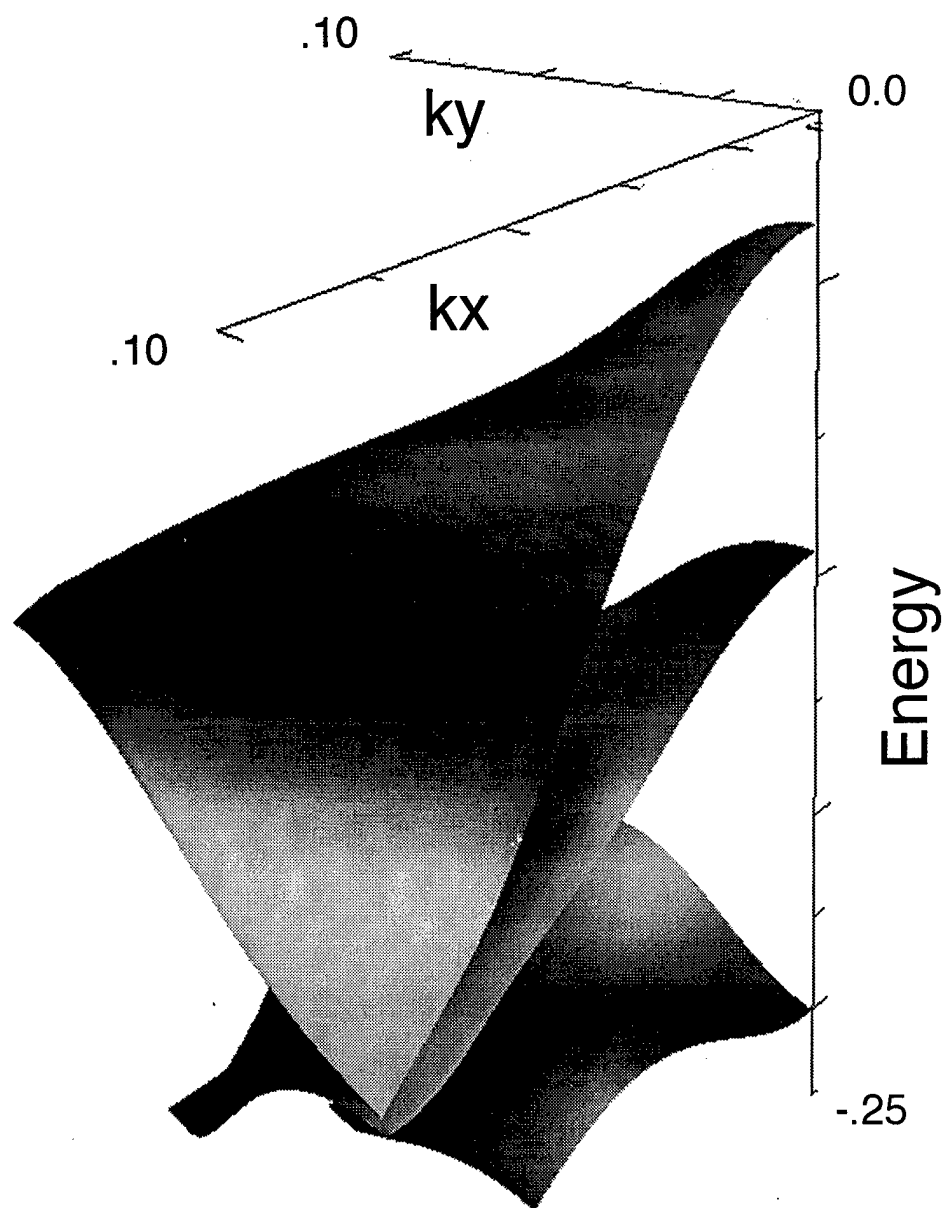


Figure 28 Surface plot of the bandstructure for [001] Si/Si₇₀Ge₃₀ quantum well with L=30 angstrom.

4.3 Anisotropy

Non-parabolic bandstructure is a result of the periodic potential created by the atomic arrangement in the crystal lattice. The atomic arrangement is not isotropic and therefore the periodicity of the potential is not isotropic. In turn, the bandstructure is not isotropic.

From the plots show in the previous section, a 90 degree azimuthal rotation in the plane of the quantum well has different results for the [110] and the [001] materials. The [001] crystals have identical bandstructures for $\theta = 0$ and $\theta = 90$. The maximum variance in the bandstructure from that at either of these values of θ occurs at 45 degrees. For the [110] materials, the anisotropy is even more significant as the bandstructure continuously changes through the entire 90 degree rotation.

The band structure in each growth direction in each type of quantum well for each type of material clearly shows an anisotropy. It can also be reasonable inferred that the anisotropy in the bandstructure is indicative of the behavior of the wave functions. Therefore calculations that require knowledge of the band structure and/or the wavefunctions, such as that of absorption coefficients, must consider this anisotropy. However, also observed from the plot is that the anisotropy is not significant for small values of k_{\parallel} . This implies that transitions dictated by the Fermi energy to be near $k_{\parallel} \approx 0$, can safely neglect the effects of bandstructure anisotropy.

4.4 Summary and Recommendations

A software package has been developed to evaluate bandstructures in semiconductor quantum wells for materials grown in both the [110] and the [001] directions. These tools have allowed analysis of the anisotropy of the quantum well bandstructure in the plane of the well.

To fully understand the magnitude of the anisotropic effects, absorption coefficients themselves should be calculated. The code generated during this research provides everything necessary to perform the calculation of the wave functions in the well. From this, the momentum matrix elements and finally the absorption coefficients can be calculated. The tools developed in this research can also be used for the generation of plots depicting Fermi surfaces. One final opportunity for further research is to include the effect of valence band and conduction band coupling by expanding the total Hamiltonian.

Appendix A. Subroutine Description

The following describes the programs and subroutines generated to perform the necessary calculations in this research.

- *EFAxxx* : This program generates a data list for plotting the determinant of the quantum well boundary condition matrix verses energy. The data list provides three records per field: energy, real part of the determinant, and the imaginary part of the determinant.
- *OFFSETxxx* : This subroutine determines the value of the constants Vb and Vw .
- *FACTxxx* : This subroutine utilizes the material constants to develop the matrix elements for the matrices making up the factored Hamiltonian, $H0$, $H1$, and $H2$.
- *KZEMATRIXxxx* : This subroutine utilizes the factored Hamiltonian matrices to develop the matrix equation describing k_z as a function of energy.
- *ORDER* : This subroutine takes the eigenvalues and eigenvectors of the $k_z(E)$ matrix and selects the linearly independent solutions. These eigenvalues are then ordered as HH , LH , LH , HH , SO , and SO . The corresponding eigenvectors are ordered in columns to create a matrix for use in the boundary condition matrix equation.
- *BCMATRIX* : This subroutine utilizes elements from the factored Hamiltonian and eigenvalue and eigenvectors of the $k_z(E)$ matrix to develop the matrix equation describing the boundary conditions for the quantum well.
- *DISPxxx* : This program calculates quantum well band structures. It incorporates a modified secant method root finder to look for roots at each step in k parallel. The output from this program is a data file containing the value of k parallel and the associated roots.

- *optionsxxxx* : This is the input data file that is read by both *EFA* and *DISP*. The options include material type, well width, number of bands, and seed values for the root finder. Only material type and well width are used in *EFA*.
- *material* : This is a data file specified in the options file. It contains stoichiometry values, Luttinger coefficients, deformation potentials, average valence band energy, etc.

Appendix B. Values for Physical Constants

The constants used in the calculations were obtained from tabulated data in People and Jackson (8) and Loehr (7).

constant	units	Si	Ge	GaAs	AlAs	InAs
Luttinger coefficients						
γ_1		4.22	13.4	7.65	3.45	19.67
γ_2		0.39	4.25	2.41	0.68	8.37
γ_3		1.44	5.69	3.28	1.29	9.29
lattice constant						
a	Å	5.431	5.658	5.654	5.6	6.0584
spin-orbit interaction term						
Δ	eV	0.044	0.29	0.34	0.28	0.38
valence band hydrostatic potential						
a_v	eV	2.1	2.00	1.16	2.47	1.00
valence band uniaxial deformation potentials						
D_u	eV	3.41	3.32	2.55	2.25	2.70
$D_{u'}$	eV	4.32	3.81	3.94	2.95	3.12
elastic constants						
C11	10^{12} Dyne/cm ²	1.675	1.315	1.1879	1.25	0.8329
C12	10^{12} Dyne/cm ²	0.65	0.494	0.5376	0.534	0.4526
C44	10^{12} Dyne/cm ²	0.801	0.684	0.594	0.542	0.396
average valence band energy						
E_{av}^v	eV	-7.03	-6.35	-6.92	-7.49	-6.67

Values for standard physical constants are given below.

Planck's constant	\hbar	J s	1.05457×10^{-34}
		ev s	6.58212×10^{-16}
Electron Mass	m_0	kg	9.10939×10^{-31}
		eV (s/Å) ²	5.68564×10^{-32}

Bibliography

1. Green, Kevin. *Theoretical Modeling of Linear Absorption Coefficient in Si/Si_{1-x}Ge_x Multiple Quantum Well Photodetectors*. Air Force Institute of Technology (AU), Wright-Patterson AFB, OH, October 1996.
2. Gregg, Michael. *Optical Absorption in Silicon-Germanium Quantum Well Structures*. Air Force Institute of Technology (AU), Wright-Patterson AFB, OH, September 1996.
3. Luttinger, J. M. and Kohn, W. "Motion of Electrons and Holes in Perturbed Periodic Fields," *Phys. Rev.* 97, 869, October 1954.
4. Hasegawa, Hiroshi. "Theory of Cyclotron Resonance in Strained Silicon Crystals," *Phys. Rev.* 129, 1029 February 1963.
5. Luttinger, J. M. "Quantum Theory of Cyclotron Resonance in Semiconductors: General Theory," *Phys. Rev.* 102, 1030 May 1956.
6. Szmulowicz, Frank and Brown, Gail J. "Calculation and Photoresponse Measurement of the Bound-to-Continuum Infrared Absorption in *p*-type GaAs/Al_xGa_{1-x}As Quantum Wells," *Phys. Rev. B* 51, 13203, May 1995.
7. Loehr, John P. *Physics of Strained Quantum Well Lasers*. Kluwer Academic Publishers, Norwell Massachusetts, 1998.
8. People R. and Jackson S. in *Semiconductors and Semimetals* 32. Academic Press, New York, 1990.
9. Saleh, B. E. A. and Teich, M. C. *Fundamentals of Photonics*. John Wiley and Sons, Inc., New York, 1991.
10. Singh, Jaspirt. *Optoelectronics, An Introduction to Materials and Devices*. McGraw-Hill Companies, Inc., New York, 1996.
11. Eppenga, R., Schuurmans, M. F. H., and Colak, S. "New *k · p* Theory for GaAs/Ga_{1-x}Al_xAs-type Quantum Wells," *Phys. Rev. B* 36, 1554, July 1987.
12. Esaki, L. and Tsu, R. "Superlattice and Negative Differential Conductivity in Semiconductors," *IBM J. Res. Develop.*, January 1970.
13. Schuurmans, M. F. H. and 't Hooft, G. W. "Simple Calculations of Confinement States in a Quantum Well," *Phys. Rev. B* 31, 8041, June 1985.
14. Robinett, R.W. *Quantum Mechanics; Classical Results, Modern Systems, and Visualized Examples*. Oxford University Press, Inc., New York, 1997.
15. Dereniak, E. L. and Boreman, G. D. *Infrared Detectors and Systems*. John Wiley and Sons, Inc., New York, 1996.

16. Rogalski, Antoni. "New Trends in Semiconductor Infrared Detectors," *Optical Engineering* 33, No. 5, May 1994.
17. Jaros, M. *Physics and Applications of Semiconductor Microstructures*. Oxford University Press, New York, 1989.
18. Kane, E. O. in *Handbook on Semiconductors*. North-Holland Publishing Company, Cambridge, Massachusetts, 1982.
19. Fox, A. M. "Optoelectronics in quantum well structures," *Contemporary Physics* 37, No. 2, 111, 1996.
20. Eisberg, R. and Resnick, R. *Quantum Physics of Atoms, Molecules, Solids, Nuclei, and Particles*. John Wiley & Sons, New York, 1985.
21. Burden, R. and Faires, J. *Numerical Analysis*. Brooks/Cole Publishing Company, New York, 1997.
22. Mitra S. S. and Massa, N. E.. in *Handbook on Semiconductors*. North-Holland Publishing Company, Cambridge, Massachusetts, 1982.
23. McKelvey, John P. *Solid State Physics for Engineering and Material Science*. Krieger Publishing Company, Florida, 1993.

Vita

Steven Novotny Jr. was born in Chicago Illinois in 1969. He grew up in Florida and attended the University of Central Florida from which he graduated Cum Laude with a B.S. in Aerospace engineering in 1992. He was also a member of the Air Force ROTC and received a commission upon graduation. He has served in the Air Force as an engineer at the Space and Missile System Center at Los Angeles AFB and in the 1st Space Launch Squadron at Cape Canaveral Air Station. He was accepted into AFIT in 1997 and graduated with an M.S. in applied physics in 1999. His wife's name is Rebeca and his sons' are Cosmo and Kepler.

Permanent address:

REPORT DOCUMENTATION PAGE			Form Approved OMB No. 0704-0188	
Public reporting burden for this collection of information is estimated to average 1 hour per response, including the time for reviewing instructions, searching existing data sources, gathering and maintaining the data needed, and completing and reviewing the collection of information. Send comments regarding this burden estimate or any other aspect of this collection of information, including suggestions for reducing this burden, to Washington Headquarters Services, Directorate for Information Operations and Reports, 1215 Jefferson Davis Highway, Suite 1204, Arlington, VA 22202-4302, and to the Office of Management and Budget, Paperwork Reduction Project (0704-0188), Washington, DC 20503.				
1. AGENCY USE ONLY (Leave blank)		2. REPORT DATE March 1999		3. REPORT TYPE AND DATES COVERED Master's Thesis
4. TITLE AND SUBTITLE Band Structure Anisotropy in Semiconductor Quantum Wells			5. FUNDING NUMBERS	
6. AUTHOR(S) Steven J. Novotny, Captain, USAF				
7. PERFORMING ORGANIZATION NAME(S) AND ADDRESS(ES) Air Force Institute of Technology 2750 P Street WPAFB OH, 45433-7765			8. PERFORMING ORGANIZATION REPORT NUMBER AFIT/GAP/ENP/99M-07	
9. SPONSORING/MONITORING AGENCY NAME(S) AND ADDRESS(ES) Gregory J. Vansuch, Major, USAF, Ph.D. Chief, Semiconductor Lasers Branch Air Force Research Lab (AFRL/DELS) 3550 Aberdeen Ave. SE Kirtland AFB, NM 87117-5776			10. SPONSORING/MONITORING AGENCY REPORT NUMBER	
11. SUPPLEMENTARY NOTES Dr. David Weeks, ENP				
12a. DISTRIBUTION AVAILABILITY STATEMENT Approved for public release; distribution unlimited			12b. DISTRIBUTION CODE	
13. ABSTRACT (Maximum 200 words) The focus of this research is an investigation of energy band anisotropy in simple quantum well structures. This anisotropy results from the asymmetry of the periodic potential within the crystal lattice. For sufficiently high doping levels, band structure anisotropy is expected to play an important role in the evaluation of the electronic and optical properties of the quantum well structures. The analysis uses a model based on a 6x6 Luttinger-Kohn k.p approach for bulk material valence band structure together with the Envelope Function Approximation. The model is used to analyze Si/SiGe, AlGaAs/GaAs, and GaAs/InGaAs quantum wells for the [001] and the [110] growth directions. The resulting bandstructures show significant anisotropy for materials grown in both the [110] and [001] directions. In all cases the materials grown in the [110] direction show a more pronounced anisotropy than the materials grown in the [001] directions. For the [001] growth directions, the bandstructures were effectively isotropic for values of k-parallel less than 0.4 inverse angstrom for Si/SiGe, 0.6 inverse angstrom for GaAs/AlGaAs, and 0.5 inverse angstrom for InGaAs/GaAs.				
14. SUBJECT TERMS Quantum wells, bandstructure anisotropy, Luttinger-Kohn k.p theory, Envelope Function Approximation, Si/SiGe, GaAs/AlGaAs, InGaAs/GaAs			15. NUMBER OF PAGES 75	
			16. PRICE CODE	
17. SECURITY CLASSIFICATION OF REPORT UNCLASSIFIED	18. SECURITY CLASSIFICATION OF THIS PAGE UNCLASSIFIED	19. SECURITY CLASSIFICATION OF ABSTRACT UNCLASSIFIED	20. LIMITATION OF ABSTRACT UL	